~~SJ-242 73-02~~

~~Limited~~

Fast Breeder Prototype Reactor "MONJU" Fuel Assembly Water Flow Test

March, 1973

NUCLEAR FUEL INDUSTRIES, LTD.

Fast Breeder Prototype Reactor "MONJU"
Fuel Assembly Water Flow Test

Abstract

This paper describes the FBR fuel assembly flow test which Power Reactor & Nuclear Fuel Development Corporation (PNC) is now developing for "MONJU".

An experiment was performed by loading fuel assembly into the water loop and the total pressure drop in the fuel assembly and its component pressure drop were measured.

The tested fuel assemblies consist of 7 reactor core fuel assemblies and 1 blanket fuel assembly. These fuel assemblies were manufactured by 5 companies as the first preproduction for "MONJU". Reactor core fuel assemblies were classified into 5 grid type spacer fuel assemblies and 2 wire wrapped spacer fuel assemblies.

The water temperature was 60°C, but one of the total fuel assembly pressure drop tests was done at 30, 40, 60 °C, and in these tests the effect of water temperature on the pressure drop was ascertained.

The Reynolds number of the investigation at the pin bundle ranged between 2.0×10^4 and 5.0×10^4 in the reactor core fuel assembly tests and between 5×10^3 and 2×10^4 in the blanket fuel assembly test. The results of the experiments have been rearranged by the Reynolds number at the pin bundle for the use of the "MONJU" design.

March, 1973

Tatsuo Kido
Yoshio Fukumitsu
Masayuki Kamiya

The work performed under contracts between Power Reactor and Nuclear Fuel Development Corporation and Nuclear Fuel Industries, Ltd.

CONTENTS

LIST OF DRAWINGS

1. Preface

THIS REPORT describes the water flow test of the Fast Breeder Prototype Reactor "MONJU" fuel assembly of which development is now being undertaken by Power Reactor & Nuclear Fuel Development Corporation (PNC).

In the designing of an atomic reactor, knowledge of flow performance of fuel assembly is one of the most important items. Above all, in the case of a fast breeder reactor fuel assembly, analysis of its flow characteristics is extremely a complex work because of the various involving factors in addition to its complex flow behavior resulting from its P/d ratio being close to 1 comparing with that of light-water reactor fuel assemblies, such as the spiral wire or grid which are employed as the fuel interval spacer, and the shape of the coolant inlet section as well as the fuel rod supporting structure which are affecting flow behavior making it more intricate.

In-water and in-sodium flow performance experiments have been conducted with JEFR fuel assemblies, and among others, with regard to pressure loss characteristics, they had demonstrated a satisfactory compatibility of both test results and reasonability of applying them after appropriate adjustment to the conventional experimental formula.

On the other part, "MONJU" fuel assemblies, which were manufactured on the basis of the designs of those organizations which participated in the design engineering of "MONJU", are not necessarily the same in their respective construction details. In this experiment, therefore, by loading into a warm-water pool a single unit of each fuel assembly designed and prepared as the first trial made fuel assembly for "MONJU" by several makers, their respective pressure loss were

measured and the necessary design data were obtained.

2. Experiments

The purpose of the experiments was to determine and grasp actual status of the flow performance of each of the fuel assemblies made and supplied for test by the participating makers, and to analyze how the difference in details of construction of those fuel assemblies would affect their flow behavior, and thus to establish a guideline for the design of the prototype reactor.

In a water model test for determination of in-sodium flow behavior, it is said that if a geometric approximation is realized and Reynold's number concurs, its approximation is satisfactory. In this water flow test, the maximum water temperature was 60°C, and by changing flow rate (volume), Reynold's number in the range of $1.4 - 5.0 \times 10^4$ was obtained. The viscous coefficient of sodium was 1.0 kg/mhr at the reactor which is about 60% of the viscous coefficient of 1.71 kg/mhr of the water of 60°C temperature. For this reason, in order to make Reynold's number close to the reactor, the test flow volume is raised up to 1,500 /min maximum. The test water is streamed into the assembly from the lower mockup plenum.

With regard to the core fuel assembly, no mockup connection tube is provided. Instead, it is of such a construction whereby the test water is directly charged from the entrance nozzle. As for the blanket fuel assembly, a shield-plate is provided in the mockup plenum and the prototype reactor is simulated so as to no streaming water enters directly into the orifice.

The subject matters of fuel assembly tests and the test conditions

are given as follows:

Table 2-1. Test Fuel Assemblies

Core Fuel Assemblies:
1. Grid type fuel assembly made by NFI (Old Sumitomo)
2. Wire type fuel assembly made by NFI (Old Sumitomo)
3. Grid type fuel assembly made by NFI (Old Furukawa)
4. " " " Mitsubishi
5. " " " Toshiba
6. Wire type fuel assembly made by Toshiba
7. Grid type fuel assembly made by Hitachi
Blanket Fuel Assembly:
1. Wire type fuel assembly made by NFI (Old Sumitomo)

The major specifications of these fuel assemblies are as follows:

Table 2-2. Major Specifications of Trial Made Fuel Assemblies

1. Core Fuel Assemblies:

* Number of fuel pins	169 pins
* Fuel pin alignment	Equilateral triangular form
* Fuel pin diameter	6.5mmϕ
* Fuel pin pitch	7.9mm
* Distance between inner walls of wrapper tube	104.3mm
* Fuel pin length	
Mitsubishi, Hitachi, NFI (Old Sumitomo)	2,795mm

NFI (Old Furukawa) 2,800mm

Toshiba 2,850mm

* Fuel assembly total length

Mitsubishi	Hitachi	Toshiba	NFI (Old Sumi-)	NFI (Old Furu-)
4,200mm	4,200mm	3,927mm	4,200mm	4,050mm

* Grid type spacer

Type	Rhombus type	Honeycomb type			
	Hitachi	Mitsubishi	Toshiba	NFI (Old Sumi-)	NFI (Old Furu-)
Number	12	15	14	15	18
Pitch	180mm	180mm	200mm	200mm	150mm
Height	26mm	15mm	15mm	15mm	15mm
Dimple number	—	3	3	6	6

* Wire type spacer

	Hitachi	Mitsubishi	Toshiba	NFI (Old Sumi-)	NFI (Old Furu-)
Diameter (mmϕ)	—	—	13, 11	1.3	—
Pitch	—	—	406mm	250mm	—

Note: Only those tested for this time are listed.

2. Blanket Fuel Assembly (NFI, Old Sumitomo)

* Fuel pin number 61 pins

* Fuel pin diameter 11.6mmϕ

* Fuel pin pitch 13.1mm

* Fuel pin length	2,797mm
* Fuel assembly total length	4,200mm
* Wire spacer and wire diameter	1.4mmϕ
	1.1mm (perimeter)
* Wire spacer pitch	300mm

2-1. Subject Matters of Test

(1) Total pressure loss characteristic test of fuel assemblies

The trial manufactured fuel assemblies were loaded into the normal temperature water test loop, and the pressure loss in the area from the entrance nozzle to the handling head was measured. The pressure loss measurement was performed by the static pressure measuring taps provided at the lower mockup plenum and on the wall of the handling head upper tube.

(2) Fuel bundle pressure loss performance test

A static pressure measuring tap was provided on the wrapper tube which was supplied by PNC, and the fuel assembly was loaded after replacing this wrapper tube with that of the fuel assembly furnished by each maker.

The measurement was performed at the two points, front and rear of the fuel bundle, and at 20 - 30 points of the entire area of fuel bundle. Thus from the results of this measurement, the pressure loss behaviors of the spacer and the fuel bundle were checked.

2-2. Test Conditions

(1) Water temperature

The streaming water temperature was 60°C. But in order to check the temperature dependency of the pressure loss, water

temperatures of 30°C and 40°C were additionally used in the test of one unit of fuel assembly during the test under Paragraph 2-1-(1).

(2) Flow volume

The core fuel assembly and blanket fuel assembly were tested and measured under the following listed flow volume:

Table 2-3. Test Flow Volume (Rate) (ℓ/min)

	Assembly's total pressure loss characteristics	Fuel bundle pressure loss characteristics
Core fuel assembly	500, 600, 700, 800, 900, 1000, 1100, 1200, 1300, 1400, 1500	500, 750, 1000 1300, 1500
Blanket fuel assembly	100, 150, 200, 250, 300, 350, 400, 450, 500	100, 200, 300 400, 500

Table 2-4. List of Pressure Loss Performance Test

		Type of Spacer	
		Wire Type	Grid Type
Core Fuel Assembly	NFI (Old Sumitomo)	Ptotal (T30, T40, T60) Pbundle (T60)	Ptotal (T60) Ptotal (T60)
	NFI (Old Sumitomo)	———	Same as above
	Toshiba	Ptotal (T60) Pbundle (T60)	Same as above
	Mitsubishi	———	Same as above
	Hitachi	———	Same as above
Blanket Fuel Assembly	NFI (Old Sumitomo)	Ptotal (T60) Pbundle (T60)	———

Note: Ptotal : Fuel assembly total pressure loss behavior test
Pbundle: Fuel bundle pressure loss behavior test
Ta : Water temperature a (°C)

3. Core Fuel Assembly Flow Performance

3-1. Test Facility and Test Section

(1) Outline of the loop and the measuring system

Fig. 1 represents the water stream loop and the block diagram of the measuring system. The pump head is 12 Kg/cm^2, and the piping of 8B and SUS 27 material.

The adjustment of the streaming water temperature is done by controling the 2ndary cooling water flow rate at the condenser and the streaming friction is used for raising of water temperature.

The streaming water temperature is limited to 70°C due to the pump's capacity demand, while the control of the flow rate is performed by the adjustment valve at the condenser's outlet.

Fig. 2 shows the block diagram of the measuring system. The pressure at each point was measured by the differential manometer - keinetic strain meter based on the standard point pressure difference, and counted and recorded by the digital printer.

The differential manometers which were used for this measuring were selected in accordance with the size of pressure loss in the range of 1.0, 5.0, and 10.0 Kg/cm^2.

The flow rate was measured by a turbine type flowmeter provided at the tube in front of the test section. The stream water temperature was measured and recorded by the C/A thermocouple installed at the immediate entrance of the test section.

Table 3-1. Measuring Instruments

	Max. measured pressure difference	Type	Allowable temp.	Maker	Pressure resistance
Differential pressure manometer	5 Kg/cm^2	Strain-meter	-5 - 65°C	Shinko Tsushin	50 Kg/cm^2
	10 Kg/cm^2	"	"	"	100 Kg/cm^2
	1 Kg/cm^2	"	"	"	10 Kg/cm^2

	Max. measured flow rate	Maker	Type	Diam.	Max. output Frequency
Flow meter	240 ton/hr	Tokiko	Turbine flowmeter	200mm	500 Hz

	Maker	Figures	Printing speed	Recording paper	Power source
Digital printer	Yokogawa Denki	13 or 19	5 lines/ sec.	No carbon paper	AC100 ± 10V

(2) Test section

Fig. 3 shows the loading of fuel assembly to the loop. The fuel assembly is sent into an eight inch test tank and is held down by means of the holding plate from floating up. The test water streams perpendicularly upward along the test section and goes through the lower mock-up and via the test section arrives at the signal extraction section. The leak from the gap or crack between the fuel assembly receiving jig and the fuel assembly when the water stream goes into the fuel assembly from the lower mockup plenum is prevented by the O-ring as indicated in the diagram. The position of the pressure gauge taps which are used for assembly's total pressure loss measuring is shown at the lower plenum and the signal extraction tube in the diagram.

These taps are silver soldered to a stainless tube of 4mmϕ (outer diameter) and 40mm long. The each end is linked with a copper tube of 6mm outer diameter and then fixed to the differential pressure manometer. The cylindrical shielding plate with holes on the wall and the flowmeter underneath were those used for the flow test of the blanket fuel assembly, and were removed for the test of this subject matter.

The following is the description of the wrapper tube which was used for the measuring of pressure loss of the fuel bundle:

This wrapper tube was leased from PNC and the pressure taps were mounted on it for the measuring of pressure distribution of fuel bundles. Fig. 6 and 7 represent respectively the detailed drawings of the location of taps mounted on a wrapper tube of 3,000mm in length.

The wrapper tube No. 1 shown in Fig. 6 was used for a series of tests of the fuel assemblies except for Toshiba fuel assembly and NFI (Old Sumitomo) wire type fuel assembly. The number of taps were set at 47 considering the spacer position of each of the assembles supplied by respective makers.

The wrapper tube No. 2 shown in Fig. 7 is for Toshiba grid type fuel assembly, and is provided with the holes for screws and taps at the positions of three equivalent intervals between Toshiba spacers. When this wrapper tube is used for a wire type fuel assembly, the screw holes are covered by pieces of copper plate by soldering. Fig. 8 - Fig. 12 show the relative positions of the pressure taps of each fuel assembly and the fuel bundles at the time of the test.

Fig. 4 and 5 show in details the hunger or swing jig and the tilting machine which were used for loading of fuel assemblies into the

test loop and for replacing the wrapper tubes. These were specially designed and manufactured to ensure the safety of the test pieces from any possible damage during the test operation.

3-2. Calibration Test of Measuring Equipment

(1) Calibration test of flowmeters

Calibration test was performed with those flowmeters which, as indicated in Table 3-1, were used in this subject test.

Fig. 13 represents the block diagram of the calibration test. This test was performed with the fuel assembly loaded to the same loop under the same condition as in the case of the flow test under water temperature at 30°C.

The test water was measured with a liquid level gauge installed in a five ton capacity water tank, and the measurement was repeated three times in the same flow rate, and the calibration was made as to a total of 14-point flow rates.

The following two points were taken into consideration to prevent the liquid surface from becoming choppy at the time of water being poured into the tank:

i) In order to make the water being sprayed evenly all over the liquid surface when water is fed from the main pipe into the tank, many small holes were made in the tubes at the upper part of the tank so that water will fall all over the surface evenly.

ii) The extraction location of the liquid level gauge was branched out into three directions so that the even value of water level can be obtained. The measurement of the water level was commended after 20 sec. - 1 min. from spraying water into

the tank. This is because when the liquid level rises, the water ripples are thought to affect less to the liquid level gauge.

Fig. 14 shows the calibration results of the flowmeter. The rectilinearity of the flowmeter's performance was satisfactory with a data input within ±0.5% for the fitting type flowmeter.

(2) Calibration test of differential manometer

Fig. 15 shows a sketch drawing of the calibration device of differential manometers. The calibration pressure was provided by water column and mercury column. The result of each differential manometer is given in Fig. 16 - Fig. 18. Each of them shows a satisfactory rectilinear performance with a data input within 0.6% for the fitting type.

3-3 Total Pressure Loss of Fuel Assembly

(1) Reynold's number dependency of pressure loss

A pressure loss measurement was performed with the wire type fuel assembly of NFI (old Sumitomo) under the stream temperatures of 30, 40 and 60 °C respectively.

From the results, the loss coefficient K was sought by the following equation:

$$K = \frac{\Delta P_{total}}{\gamma V^2 / 2g} \qquad (1)$$

Here,

ΔP_{total} : Total pressure loss of fuel assembly.

γ : Hydraulic specific gravity volume.

V : Mean flow velocity at the fuel assembly.

g : Acceleration of gravity.

It has been said that when a channel's configuration is in the same dimension, K will become the function of Reynold's number alone. K calculated by the equation (1) was plotted relating to Reynold' number Re and is shown in Fig. 19.

Here, Reynold's number Re is defined by the following equation:

$$Re = \frac{V \cdot De}{\nu} \qquad (2)$$

Here,

De : Fuel bundle equivalent diameter.

ν : Keinetic viscosity coefficient.

Then, $K = a\,Re^{b}$ (8)

When K obtained by the experiment is fitted with the equation (3), it is:

$$K = 168.8\ Re^{-0194} \pm 0.7\% \qquad (4)$$

and the results of 30, 40 and 60 °C are unified by the equation (4) within the accuracy of 0.7%. This well suggests the reasonability of the water model test of the sodium flow performance having different viscosity coefficients.

(2) Loss coefficient

Fig. 20 and 21 show the pressure loss measurement results and the loss coefficient of each of the fuel assemblies supplied by respective makers.

In this test, though the mockup of the complex flow pattern at the entrance nozzle is not sufficnent, the pressure loss at this point was so small that the difference by the type of spacer of each maker and by

the number of spacer are very well demonstrated in the measured results.

It was particularly noted that the pressure loss of the assembly of the grid type spacer was greater than in the case of the wire type.

The reason for smaller total pressure loss of the wire type fuel assembly in the case of NFI (old Sumitomo) which had more number of spacer binding compared with that of Toshiba was that the former had no neutron shielding block built into the assembly.

The following table shows the results of the pressure loss coefficients of each of the fuel assemblies of various makers expressed by Reynold's numbers at the fuel elements:

Table 3-2. Correlation Equations of Total Pressure Loss Coefficients of Fuel Assembly

	Assembly	Correlation equation of pressure loss coefficient
Grid Type	NFI (Old Furukawa)	$K = 350 \quad Re^{-0.159} \pm 0.4\%$
	NFI (Old Sumitomo)	$K = 208.4\ Re^{-0.160} \pm 0.6\%$
	Toshiba	$K = 244.4\ Re^{-0.165} \pm 0.5\%$
	Mitsubishi	$K = 253.6\ Re^{-0.167} \pm 0.6\%$
	Hitachi	$K = 196.2\ Re^{-0.175} \pm 0.6\%$
Wire Type	Toshiba	$K = 217.2\ Re^{-0.216} \pm 0.5\%$
	NFI (Old Sumitomo)	$K = 168.8\ Re^{-0.194} \pm 0.5\%$

The following shows the cross section and the corresponding diameter of the channel at the fuel bundle section used in the operation of the above equation:

Table 3-3. Channel's Cross Section and Corresponding Diameter

	Grid type (Excluding Hitachi)	Hitachi grid type	Wire type
Channel cross section	38.67cm^2	37.60cm^2	35.42cm^2
Correspoding diameter	0.4055cm	0.3712cm	0.3146cm

3-4 Pressure Loss at Fuel Bundles

(1) Grid type fuel assembly

As shown in Fig. 8 - Fig. 12, the pressure distribution of each fuel assembly was measured at one or two points of each spacer interval including both the inlet and outlet of the fuel bundle. From the pressure measurement results at these positions, the spacer loss coefficient and the friction loss coefficient were respectively sought in the following manner:

i) Spacer and friction loss coefficients

Fig. 22 - Fig. 26 show the results of pressure loss measurement at the fuel bundle section. Here, in Fig. 22, the mean value of the pressure losses at the front and rear of the spacers of Toshiba fuel assembly only, and as to other assemblies, the pressure loss at each measuring point was indicated taking one pressure tap at the lower part of fuel bundle as a criterion. According to the measurement results of Toshiba fuel assembly, the pressure difference at 13.3cm interval with the spacer at the center is almost the same within ±2% with all the spacers. Fig. 22 represents the plotted diagram of the mean value of the pressure difference

(= pressure loss) against each measured flow volume. From this, each spacer pressure loss can be considered as uniform regardless of positions in the axial direction, and by the following procedure, the friction loss coefficient was computed:

$$\Delta Pn = \frac{\gamma}{2g} V^2 \left(\frac{\ell n}{De} \cdot f + mK \right) \qquad (1)$$

The equation (1) shows the pressure loss from the standard tap position to the tap position at n.

Here,

γ : Stream specific gravity volume

V : Mean stream velocity at fuel bundle

ℓn : Length from the standard position

De : Corresponding diameter

m : Number of spacers up to n

f : Friction loss coefficient

K : Spacer loss coefficient

Table 3-5 - Table 3-8 represents part of the results derived by obtaining f, K by hypothetically establishing the equation (1) and processing the measured data by the method of least squares. The residual shown in the table is the difference of the calculated values of pressure loss computed from f, K obtained by the experimental data and is expressed by the following formula:

$$\text{Residual} = \left(\frac{\text{Calculated value - Experimental value}}{\text{Experimental value}} \right) \times \text{Pressure loss} \qquad (2)$$

Looking at the results, except for the neighbouring of the standard point where measuring accuracy deteriorates, residual is within 2 - 3% showing the reasonability of the equation (1).

K and f obtained by the above method are respectively shown in Fig. 27 and 28. As shown in the diagrams, the spacer loss coefficient are approximately uniform without relation to Reynold's number, while the friction coefficients are the gradient to -0.19 to -0.25 powers of Reynold's number Re. The spacer loss coefficient distribution was in the range of 1.1 - 1.9 with the honeycomb type, while with the diamond shaped lattice type spacer, it was noted at a low figure of 0.6. The reason that the honeycomb type spacer of NFI (old Furukawa) is higher and that of Mitsubishi is lower is thought because the thickness of the plate which forms the unit cell of the former is 0.2mm which is thicker by 0.05mm than that of NFI (old Sumitomo) and Toshiba, and also because the latter has no triangular obstacle on the grid periphery.

The friction loss coefficient, although shows against Re number almost the same trend as Clausius method, is rather low by some 10% as a whole.

ii) Pressure loss at the fuel bundle spacers

From the measured value of the pressure difference of the taps provided at the fuel bundle entrance and the lowest end of the fuel bundle, the pressure loss at the support structure at the lower end of the fuel bundle was sought, of which results

are shown in Fig. 30. As for each fuel assembly, the fuel element is fitted to the knock-bar or the grid, and the fuel bundle is fixed to the entrance nozzle via either a framework of a shielding block.

The diagram shows for reference the plotted pressure loss at each single spacer obtained by i). From this result, it can be seen that the pressure loss at the grid type support is about 1.4 times larger than at the honeycomb type spacer. While the knock-bar type support shows a pressure loss of 1/2 - 1.0 times larger than the honeycomb type spacer.

iii) Total pressure loss at the fuel bundle

Fig. 29 shows the total pressure loss at the fuel bundle measured from the tap at the fuel bundle entrance. Reynold's number was computed based on the stream velocity at the fuel section. Hitachi's grid type, having an outer fuel rod (stainless rod of 1.8ϕ outer diameter), is smaller in equivalent diameter than its counterparts of other makers, its pressure loss as shown in the diagram is close to that of Mitsubishi. But considering on the basis of assembly's flow volume, it is 1,500 ℓ/min, and its difference from Mitsubishi is about 1.0 Kg/cm^2.

(2) Wire type fuel assembly

Fig. 31 and 32 show the results of measurement of the wire type fuel assembly.

The pressure loss at the fuel bundle area shows an increase in proportion to the length of the fuel section.

Fig. 33 shows the pressure loss of fuel bundles of 2,755mm of

both NFI (old Sumitomo) and Toshiba.

When the pressure loss coefficient is adjusted as 3-3 (1), and is expressed by Reynold's number, it is as follows:

NFI (old Sumitomo): $K = 128.3\ Re^{-0.186} \pm 0.7\%$

Toshiba: $K = 161.0\ Re^{-0.224} \pm 0.4\%$

3-5 Pressure Loss at Structures Other Than Fuel Bundles

By substracting the total fuel bundle pressure loss from the total fuel assembly pressure loss, it was compared with the pressure losses at the neutron shield block and other areas. The results are represented by Fig. 34.

NFI (old Sumitomo), having no neutron shield block built in, showed the lowest figure. NFI (old Furukawa) showed the highest figure, which is considered due to the large wetted perimeter of the blocks in the handling head and the entrance nozzle.

The following table indicates the ratio of this loss against the total loss:

Pressure Loss Share Ratios of Structures Other Than Fuel Bundles

(Table 3-4)

Assembly	Pressure loss share ratio
NFI (old Sumitomo)	12 ± 1.0%
NFI (old Furukawa)	28 ± 0.3%
Mitsubishi	19 ± 0.5%
Hitachi	22 ± 0.3%
Toshiba	18 ± 0.5%

Table 3-5. Pressure Loss Coefficient Calculation Results

(Mitsubishi Grid)

Flow rate: 1,500 ℓ/min.

Spacer loss coefficient = 1.124 Friction loss coefficient = 0.01648

Pressure loss (Experiment)	Pressure loss (Calculation)	Residual
0.354	0.318	-0.102
0.423	0.369	-0.129
0.760	0.720	-0.052
0.842	0.788	-0.064
1.101	1.072	-0.026
1.202	1.156	-0.038
1.514	1.487	-0.018
1.578	1.542	-0.023
1.856	1.834	-0.012
1.966	1.927	-0.020
2.271	2.253	-0.008
2.333	2.304	-0.012
2.656	2.639	-0.006
2.767	2.732	-0.013
2.990	2.999	0.003
3.127	3.109	-0.006
3.410	3.410	-0.000
3.504	3.486	-0.005
3.752	3.761	0.003
3.892	3.888	-0.001
4.144	4.172	0.007
4.253	4.248	-0.001
4.558	4.574	0.004
4.652	4.659	0.001
4.909	4.951	0.009
5.057	5.044	-0.003
5.308	5.337	0.005
5.420	5.421	0.000
5.694	5.731	0.006

Table 3-6. Pressure Loss Coefficient Calculation Results

(Hitachi Grid)

Flow rate: 750 ℓ/min.

Spacer loss coefficient = 0.637 Friction loss coefficient = 0.02254

Pressure loss (Experiment)	Pressure loss (Calculation)	Resident
0.018	0.020	0.120
0.092	0.089	-0.033
0.112	0.109	-0.026
0.198	0.191	-0.033
0.226	0.218	-0.034
0.279	0.274	-0.019
0.309	0.307	-0.006
0.381	0.381	0.000
0.402	0.403	0.002
0.480	0.479	-0.003
0.499	0.499	-0.001
0.570	0.571	0.002
0.588	0.591	0.005
0.668	0.667	-0.002
0.714	0.717	0.004
0.794	0.796	0.002
0.849	0.853	0.005
0.920	0.922	0.002
0.971	0.976	0.004
1.057	1.058	0.001
1.110	1.112	0.001
1.193	1.190	-0.002
1.233	1.231	-0.002
1.317	1.313	-0.003

Table 3-7. Pressure Loss Coefficient Calculation Results
(Sumitomo Grid)

Flow rate: 1,003 ℓ/min

Spacer loss coefficient = 1.42 Friction loss coefficient = 0.0202

Pressure loss (Experiment)	Pressure loss (Calculation)	Residual
0.018	0.028	-0.557
0.224	0.236	-0.052
0.260	0.273	-0.050
0.429	0.434	-0.011
0.467	0.471	-0.009
0.646	0.655	-0.014
0.686	0.702	-0.023
0.873	0.865	0.009
0.902	0.896	0.007
1.103	1.084	0.017
1.313	1.297	0.012
1.340	1.325	0.011
1.532	1.514	0.012
1.548	1.537	0.007
1.743	1.716	0.015
1.770	1.740	0.017
1.993	1.947	0.023
2.180	2.145	0.016
2.219	2.197	0.010
2.386	2.348	0.016
2.411	2.376	0.014
2.618	2.575	0.017
2.649	2.603	0.018
2.764	2.815	-0.018
2.973	2.999	-0.009
3.004	3.032	-0.009
3.187	3.211	-0.008
3.240	3.253	-0.004

Table 3-8. Pressure Loss Coefficient Calculation Results

(Furukawa Grid)

Flow rate: 1,007 ℓ/min.

Spacer loss coefficient = 1.71 Friction loss coefficient = 0.0172

Pressure loss (Experiment)	Pressure loss (Calculation)	Residual
0.023	0.024	0.046
0.227	0.226	-0.006
0.150	0.147	-0.019
0.466	0.467	0.003
0.679	0.685	0.009
0.892	0.907	0.017
1.101	1.121	0.018
1.309	1.330	0.016
1.334	1.354	0.015
1.534	1.560	0.017
1.557	1.584	0.017
1.734	1.770	0.021
1.777	1.814	0.021
1.973	1.999	0.013
2.002	2.035	0.017
2.200	2.229	0.013
2.435	2.459	0.010
2.646	2.660	0.005
2.685	2.700	-0.006
2.901	2.886	-0.005
2.938	2.922	-0.005
3.136	3.104	-0.010
3.165	3.128	-0.012
3.377	3.329	-0.014
3.404	3.358	-0.014
3.638	3.563	-0.021
3.665	3.591	-0.020
3.851	3.777	-0.019
3.890	3.809	-0.021

4. Blanket Fuel Assembly Flow Characteristics

4-1. Experimental Loop and Test Section

The loop and the measuring system are the same as described in Section 3.

As the detailed drawing of the test section is represented by Fig. 3, it is of such a construction that a stream shield plate is provide in the lower mockup plenum so that the test water will not directly stream into the assembly orifice.

For the measuring of the fuel bundle pressure loss behavior, a wrapper tube No.2 as shown in Fig. 6 was employed. The taps which were employed for pressure gauging are shown in Fig. 35.

4-2. Measuring Instruments

(1) Differential Manometer

The same instrument as described in Section 3 was employed.

(2) Flowmeter

TOKIKO's turbine flowmeters of the maximum capacity of 90 ton/hr were employed. Flow calibration was entrusted with the Weight and Measure Research Institute of the Ministry of International Trade and Industry. The results are shown in Table 4-1.

4-3. Pressure Loss

Fig. 36 represents the total pressure loss of the fuel assembly and the total fuel bundle pressure loss. The total fuel assembly pressure loss was 1.75 Kg/cm^2 under the flow volume of 500 /min., and the data were riding on the line of 1.9 power of Reynold's number at the fuel section.

The reason for the stronger gradient of the assembly's total

pressure loss against Reynold's number compared with the pressure loss at the fuel bundle section is considered due to the effect of the orifice.

Fig. 37 represents the pressure difference distribution at the fuel bundle section. The same as the wire type fuel assembly described in Section 3, the pressure loss shows a rectilinear increase in proportion to the fuel length.

5. Results of Study

5-1. Pressure loss at Fuel Bundle

The measured results of the fuel bundle pressure loss were correlated and summarized by the method proposed by Klaus Rehme*1 and subsequently a comparative study of the spacer pressure loss was performed.

Klaus Rehme conducted an experiment of both the grid type and the wire type spacers in a water pool. The test specimen length was 1,500 mm, and changed the fuel bundle P/D to 1.125 - 1.417 and also to the range of 7 - 169 when the number of fuels were aligned in a triangular shape.

As to the test specimen spacers, the several types of spacers including the grid type, honeycomb type, diamond type, etc., were made into a configuration parameter.

As to the wire type, the spacer pitch, the diametric ratio (H/dm) and the number of fuel elements were parametrically converted to 6-45 and 7-61 respectively. The experimented Reynold's number was within

*1 "Literature: Pressure Drop Correlations for Fuel Element Spacers" Kalus Rehme nuclear tech. vol. 17, Jan. '73.

the range of 10^3 - 3×10^5 on the basis of the fuel element section.

The results of these experiments, the spacer's projected cross section in the case of the grid type, and the wetted perimeter of the wrapper tube and its effective speed in the case of the wire type were respectively introduced and rearranged to provide them a revised loss coefficient. This result has uniformed the several spacer parameters, and has been compared and correlated with other previous experimental data.

(1) The grid type spacer loss coefficient

The grid type spacer loss coefficient K obtained in Section 3-4 is rearranged as follows:

$$K = C \times \left(\frac{Av}{As}\right)^2 \qquad (1)$$

Here,

C : Modified loss coefficient

Av: Projected grid cross section

As: Undisturbed flow section

The reason for the introduction of Av, As is that the pressure loss at the spacer section is because of the stream restraint mainly at the spacer cross section and the spacer section. Fig. 38 shows C computed by the equation (1). Most of the data of the honeycomb type spacer, about 90%, is in the range of 13 - 11 which is somewhat a diminished function against Reynold's number. By contrast, with with rhombus type spacer, C is in the range of 13.5 - 10 which is rather a larger gradient against Reynold's number. With these two spacer types, although there is seen the above mentioned difference, it can be regarded as the revised loss coefficients being conforming within ± 5%.

On the other hand, with Klaus Rehme, it is although the same as the results of this experiment in respect of the conformity of the revised loss coefficients of both types of spacers and Reynold' number dependency, the values are in the range of 6 - 8. The revised loss coefficient obtained as the result of this experiment is about 1.7 times as high as that of Klaus Rehme. As to the difference of the absolute value of the revised loss coefficient, the similar case is also reported in Literature *1, in which the experimental value of Spengos *2 is higher than that of Klaus Rehme by a 1.5 - 1.8 level.

This difference, Klaus Rehme attributed to the difference of the number of spacers which support the fuel bundle (4 in the case of Spengos.)

As the details of the experiment of Klaus Rehme are unknown, it is difficult to determine the state of the test specimen. But the difference in the revised loss coefficient is considered due to the difference in the flow performance arising from the different space interval and position.

At any rate, in respect of the fuel assembly for the prototype reactor core, it has been determined that, from the friction loss coefficient obtained by 3 - 4 and the spacer's cross section, the pressure loss estimation can be deduced with a considerable accuracy.

The projected cross sections of spacers of respective makers are given in the following table:

---

*2 Literature: "Tests on Model of Nuclear Reactor Elements. IV. Model Study of Fuel Element Supports."

C. Spengos UMRI - 2431 - 4P, Univ. of Michigan Research Institute, Ann Arbor ('59).

Table 5-1. Projected Cross Section of Each Spacer (cm^2)

NFI (Old Sumitomo)	NFI (Old Furukawa)	Toshiba	Mitsubishi	Hitachi
13.86	14.63	13.86	11.71	9.10

(2) The wire type spacer pressure loss coefficient

The measured values of the pressure loss at the fuel bundle section of NFI (old Sumitomo) and Toshiba wire type core fuel assemblies as well as of NFI (old Sumitomo) blanket fuel assembly were rearranged by Klaus Rehme's method. The pressure loss of the wire type spacer is expressed by the following equation the same as the friction loss correlation equation:

$$\Delta P = f \cdot \frac{\gamma}{2g} V^2 \cdot \frac{L}{De} \qquad (1)$$

Here,

De : Equivalent diameter ($4A^t/St$)

At: Flow area
St: Total length of the wetted perimeter (including the wrapper tube)

L : Fuel bundle length

V : Flow velocity

γ : Specific gravity volume

f : Pressure loss coefficient

The ratio which the sub-channel in the perimeter of the channel of smaller resistance occupies in the loss coefficient f as above defined against the entire length of the wetted perimeter, and the effective loss coefficient f' which is shown by the following equation by introducing the effective flow velocity of the coolant which streams along the

wirewrap are defined as follows:

$$f' = \frac{f}{F}\,\frac{St}{Sb} = \frac{\Delta P}{\frac{\gamma}{2g}\,\frac{L}{De}\,V^2 F} \cdot \frac{St}{Sb} \qquad (2)$$

$$F = \left(\frac{P}{D}\right)^{0.5} + \left[7.6\,\frac{dm}{H}\left(\frac{P}{D}\right)^2\right]^{2.16} \qquad (3)$$

Here,

F : $\left(\frac{\text{Effective flow velocity}}{\text{Mean flow velocity}}\right)^2$

P : Fuel pin pitch

D : Fuel pin diameter

bm : Wire diameter

H : Wire pitch

Sb : Wetted perimeter of fuel pin and wire

The revised friction coefficient of the equation (2) was calculated with respect to the wire type fuel bundle which was tested during this experiment, and the result of the plot made of the modified Reynold's number is shown in Fig. 39.

Here, the modified Reynold' number is by the effective flow velocity and is expressed by the following equation:

$$Re' = Re\,\sqrt{F} \qquad (4)$$

Here,

Re : Reynold's number by the mean flow velocity.

Fig. 5-2 provides both the modified friction coefficients and the correlation equations obtained by Klaus Rehme. As the diagram is self-explanatory, the measured results concur within ±5% with the figures of Klaus Rehme. The wire pitch effectiveness in Klaus Rehme is expressed by H in the equation (3).

With regard to the core fuel assemblies, monitoring was performed with those having wire pitch of 406mm and 250mm respectively, and when the modified loss coefficients calculated from the measured values of both pitches were compared, there was systematically a difference of 10%. This, when calculated by the equation (3), the difference of F in the spacer pitch of 406mm and 250mm was very little and the difference of pressure loss calculation value was about 1%, while by the actual measured value, it had a difference of 10%.

5-2. Reasonability of Water Model Test

Relating to the reasonability of water model test for grasping sodium flow performance, there is a report by Ishibashi and Himeno on an experiment with use of JOYO fuel assembly. According to the report, when the changes by time lapse during sodium flow are ignored, the flow performances of water and sodium are said to concur within the experimental accuracy if Reynold's number is matched with.

In this flow test, a study was made as to the effect of density and viscosity coefficient of water upon the pressure loss performance under the varied water temperatures of 30, 40, and 60 $^{\circ}$C.

The results showed as related in Paragraph 3-3-(1) a concurrence of the pressure loss coefficient under each temperature with Reynold's number within 1% range.

This shows that the pressure loss performance is controlled by Reynold's number, and also suggests the reasonability of sodium simulation in this flow test.

6. Postscript

The results of the water flow test are summarized as follows:

(1) Total pressure loss performance of fuel assemblies

The total pressure loss is greater with the grid type fuel assembly than the wire type assembly. The measured values of the pressure loss of assembly's flow volume of 1,300 ℓ/min (Reynold's number 4.8×10^4) are 5 - 9.7 Kg/cm^2 with the grid type and 4 Kg/cm^2 with the wire type. The pressure loss difference of the grid type has as a major factor the type and number of the spacers.

The pressure loss coefficient can be fitted within 1% by the function of Reynol's number. The pressure loss coefficient of the grid type is -0.16 - 0.175 power of Reynold' number and with the wire type, it is a function of -0.2 power. The results under the varied temperatures of 30, 40 and 60 $^{\circ}C$, the pressure loss coefficient concurred with Reynold's number within 1%. This means that the pressure loss performance can be regulated by Reynold's number.

(2) Fuel bundle pressure loss performance

The pressure loss coefficient of the grid type spacer maintained a given value relating to Reynold's number in the case of the honeycomb type, while in the case of the rhombus type, it became a diminution function.

With the honeycomb type, the pressure loss coefficient formed the following values due to the difference in the plate thickness of the unit cell and the existance of the triangular obstacles in the cell perimeter.

Spacer Pressure Loss Coefficient (Honeycomb Type)

		Unit Cell Plate Thickness	
		0.15 mm	0.20 mm
Triangular Obstacle	Yes	1.50	1.80
	No	1.05	——

On the other hand, the pressure loss coefficient of the rhombus type spacer was 0.64, which concurred with other makers' spacers within ± 5% when disposed by the spacer's cross section and the channel cross section using the method proposed by Klaus Rehme, and the modified loss coefficient is calculated.

The friction loss coefficient at the elementary tube section declined by -0.20 to -0.25 power of Reynold's number, and its value showed about 10% lower value against Clausius method.

The measured value of pressure loss at the wire type fuel bundle and the calculated value by the method of Klaus Rehme concurred within ± 5%.

(3) Pressure loss characteristics at fuel bundle supports and other structures

The pressure loss at the fuel bundle support was sought by compensating the channel cross section with the measured values of the static pressures at the two points with a fuel bundle support in between.

The pressure loss coefficient with the flow velocity at the fuel bundle as the basis was as follows:

Grid type support	2.2
Knock bar support	0.68 - 1.1

The pressure loss coefficients of the neutron shielding block, handling head and others were sought by substracting the fuel assembly total pressure loss. The ratio of pressure loss at this section against the fuel assembly total pressure loss was about 20%.

For the purpose of reference, the measured values of pressure loss at each section and their respective share ratios against the fuel assembly total loss are represented in Table 6-1.

Table 6-1. Pressure Loss at Assembly Composition Elements and Pressure Loss Share Ratios

	Items / Makers	Assembly Total Pressure Loss Kg/cm²	Fuel Bundle Section							Handling Head Neutron Shield Entrance Nozzle		Assembly Flow Rate (60°C)
			Elementary Tube Sec.		Spacer Sec.		Fuel Bundle Support		Pressure Loss (kg/cm²) / Bundle Length (cm)			
			P L (Kg/cm²)	Ratio (%)	P L (Kg/cm²)	Ratio (%)	P L (Kg/cm²)	Ratio (%)		P L (Kg/cm²)	Ratio (%)	
Grid Type Fuel Assembly	NFI (Old Furukawa)	9.84	1.76	17.9	4.94	50.2	0.36	3.6	0.0253	2.78	28.3	1300 (ℓ/min)
	NFI (Old Sumitomo)	6.73	2.03	30.2	3.48	51.7	0.38	5.5	0.0211	0.85	12.6	
	Toshiba	6.59	2.15	32.6	3.21	48.7	0.10	1.5	0.0192	1.13	17.2	
	Mitsubishi	5.71	1.99	34.9	2.52	44.1	0.09	1.6	0.0163	1.11	19.4	
	Hitachi	4.97	2.47	49.7	1.17	23.6	0.23	4.6	0.0138	1.10	22.1	
Wire Type Fuel Assembly	NFI (Old Sumitomo) Core Fuel	4.05	Fuel element pressure loss 3.35 Kg/cm² Share ratio 82.7 %				0.09	2.2	0.0118	0.61	15.1	
	Toshiba Core Fuel	4.17	Fuel element pressure loss 3.03 Kg/cm² Share ratio 72.7 %				0.09	2.1	0.0106	1.05	25.2	
	NFI (Old Sumitomo) Blanket Fuel	1.71	Fuel element pressure loss 0.67 Kg/cm² Share ratio 39.2%				0.04	2.3	0.0023	1.00	58.5	500 (ℓ/min)

Fig. 1. Loop, Measurement System Flow Sheet

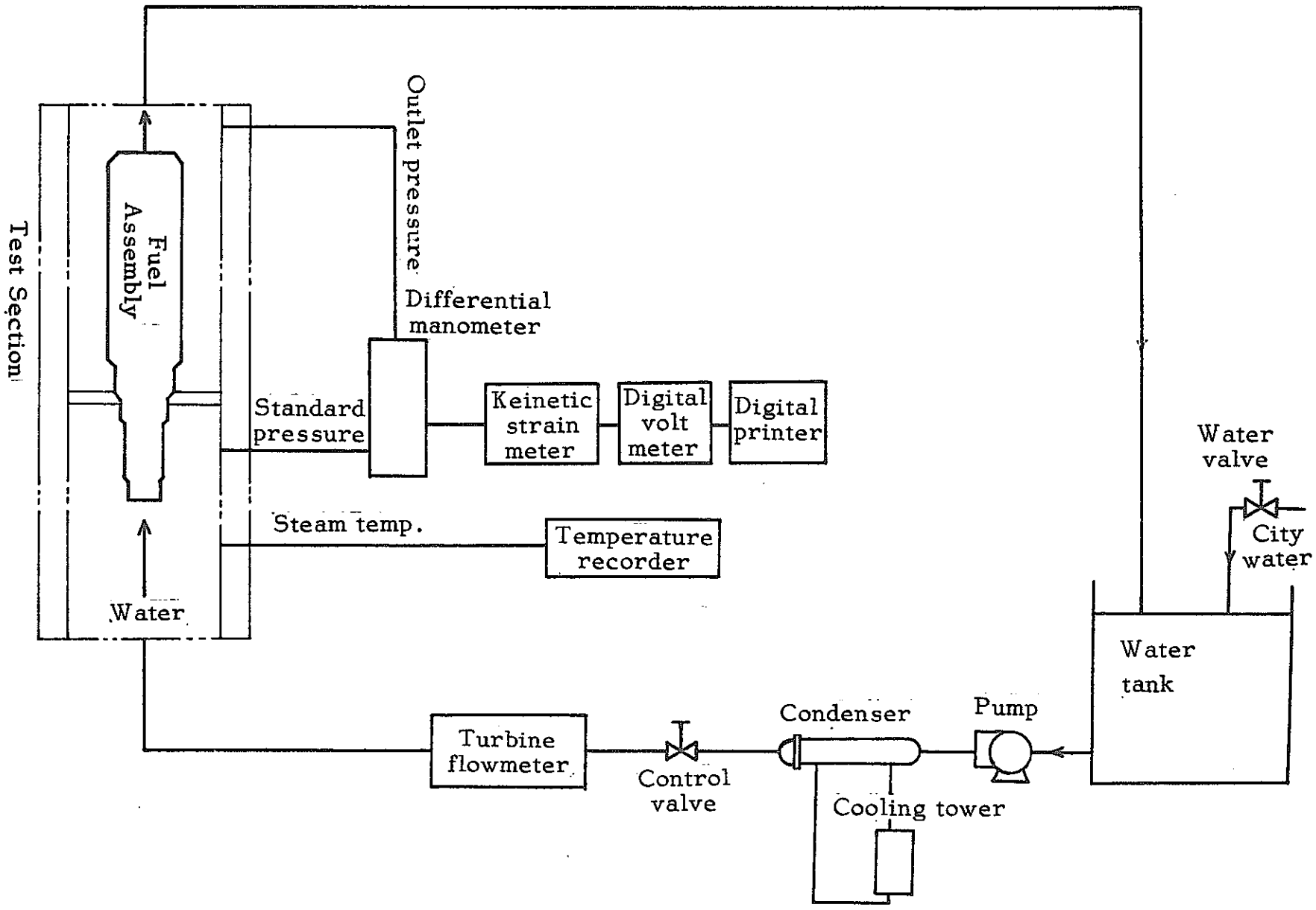

Fig. 2. Measurement System Block Diagram

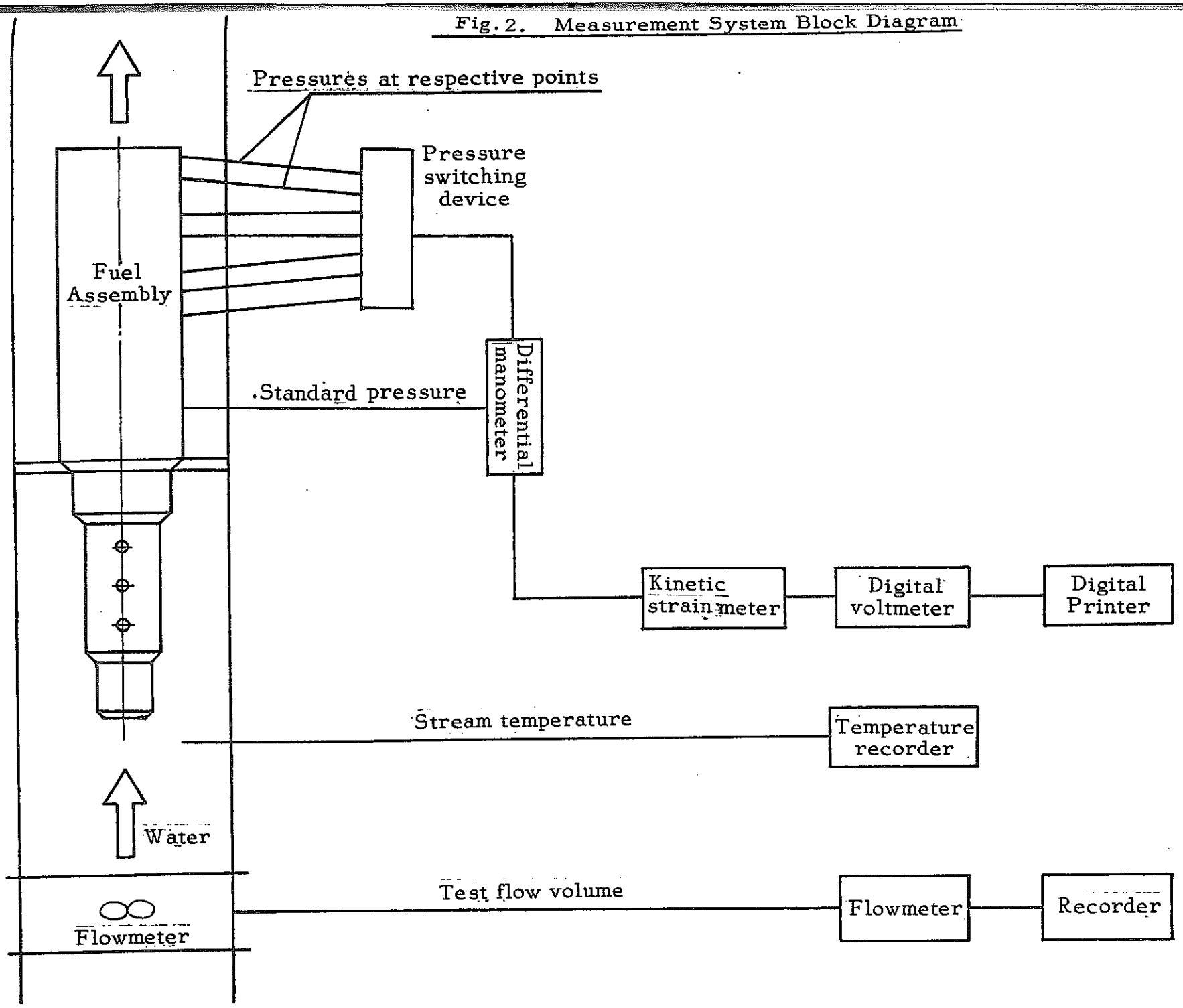

Fig. 3 Test Tank Assembly Drawing

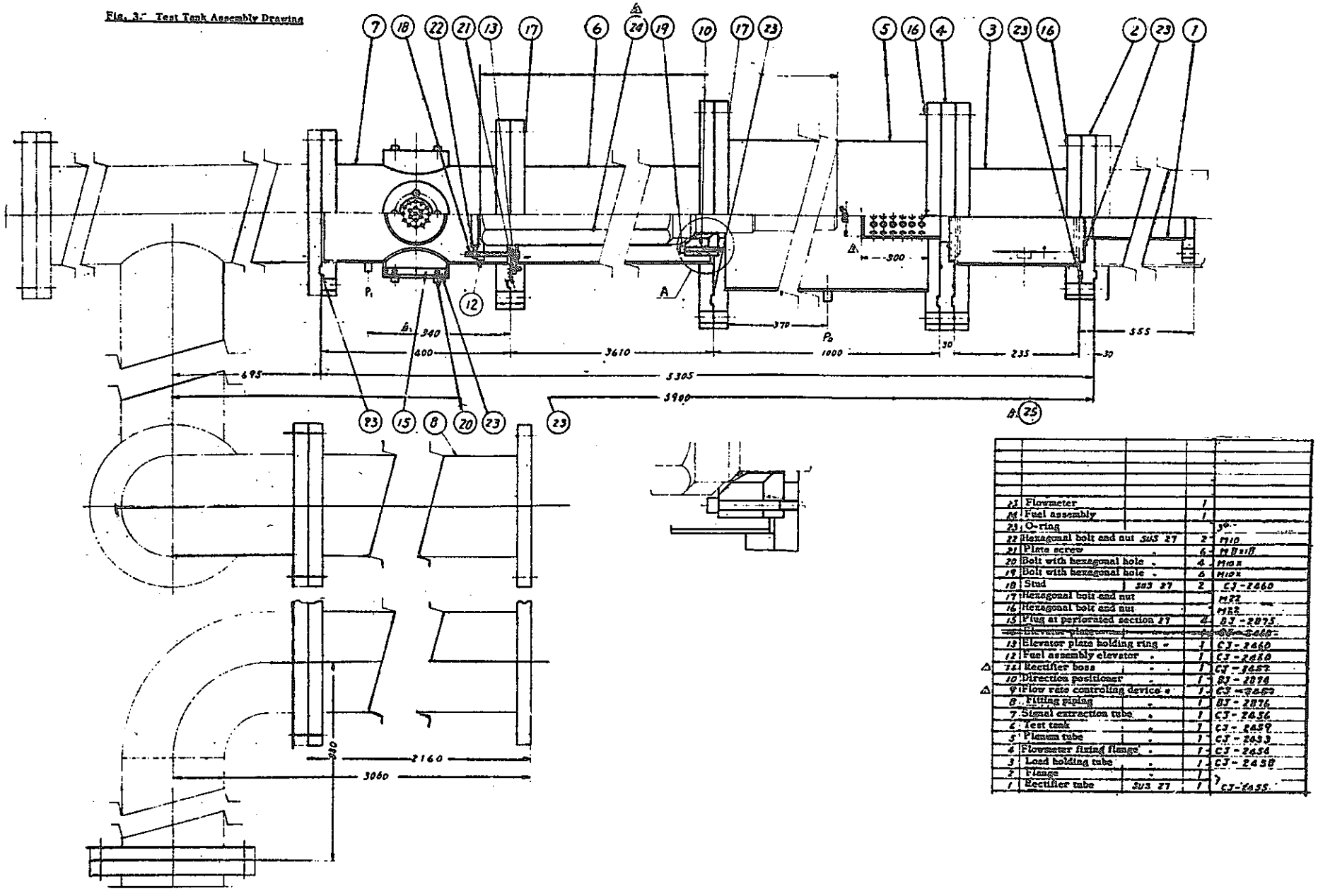

25	Flowmeter		1	
24	Fuel assembly		1	
23	O-ring		5	
22	Hexagonal bolt and nut	SUS 27	2	M10
21	Plate screw		6	M8×18
20	Bolt with hexagonal hole		4	M8×8
19	Bolt with hexagonal hole		6	M10×8
18	Stud	SUS 27	2	CJ-2460
17	Hexagonal bolt and nut			M22
16	Hexagonal bolt and nut			M22
15	Plug at perforated section	27	2	BJ-2875
14	Elevator plate		1	CJ-2460
13	Elevator plate holding ring		1	CJ-2460
12	Fuel assembly elevator		1	CJ-2460
△ 11	Rectifier boss		1	CJ-2457
10	Direction positioner		1	BJ-2876
△ 9	Flow rate controlling device		1	CJ-2459
8	Fitting piping		1	BJ-2876
7	Signal extraction tube		1	CJ-2456
6	Test tank		1	CJ-2459
5	Plenum tube		1	CJ-2453
4	Flowmeter fixing flange		1	CJ-2454
3	Load holding tube		1	CJ-2458
2	Flange		1	CJ-2455
1	Rectifier tube	SUS 27	1	

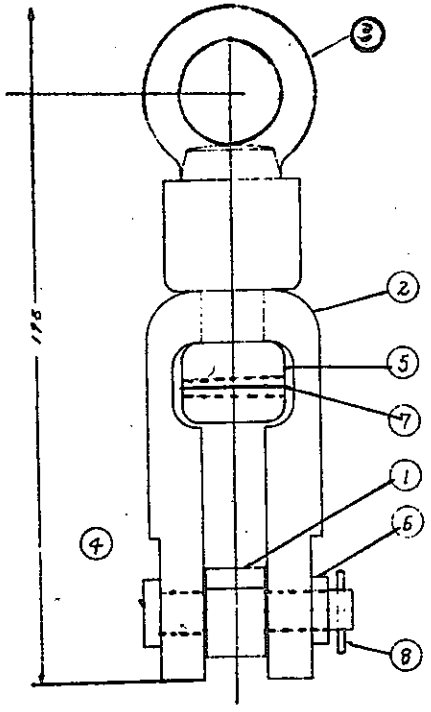

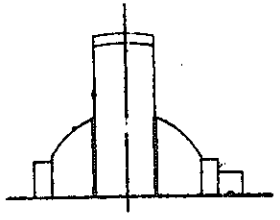

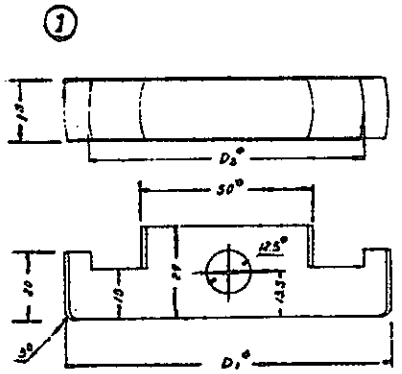

	D_1°	D_2°
A	93	81
B	92	84
C	88	87

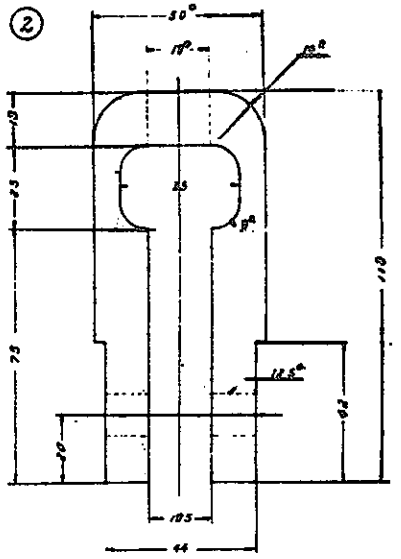

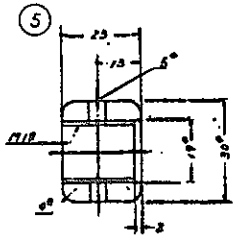

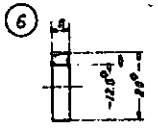

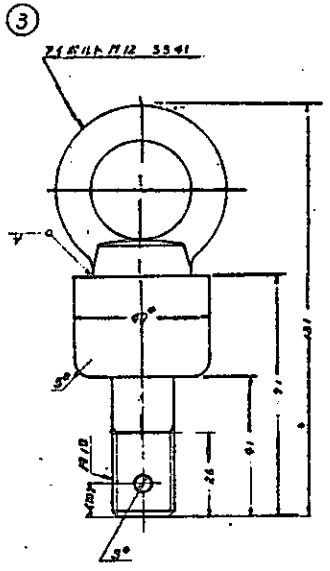

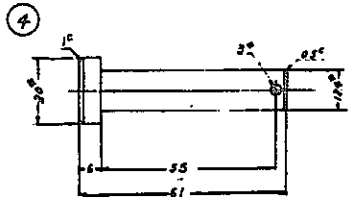

	8			Split pin		SUS 304	
	7			Taper pin		"	
	6			Collar		"	
	5			Ring nut		"	
	4			Pin		"	
	3			Swing jig		"	
	2			Jig body		"	
	1			Hook		SUS 304	
A	B°			—			

Fig. 4. Swing jig

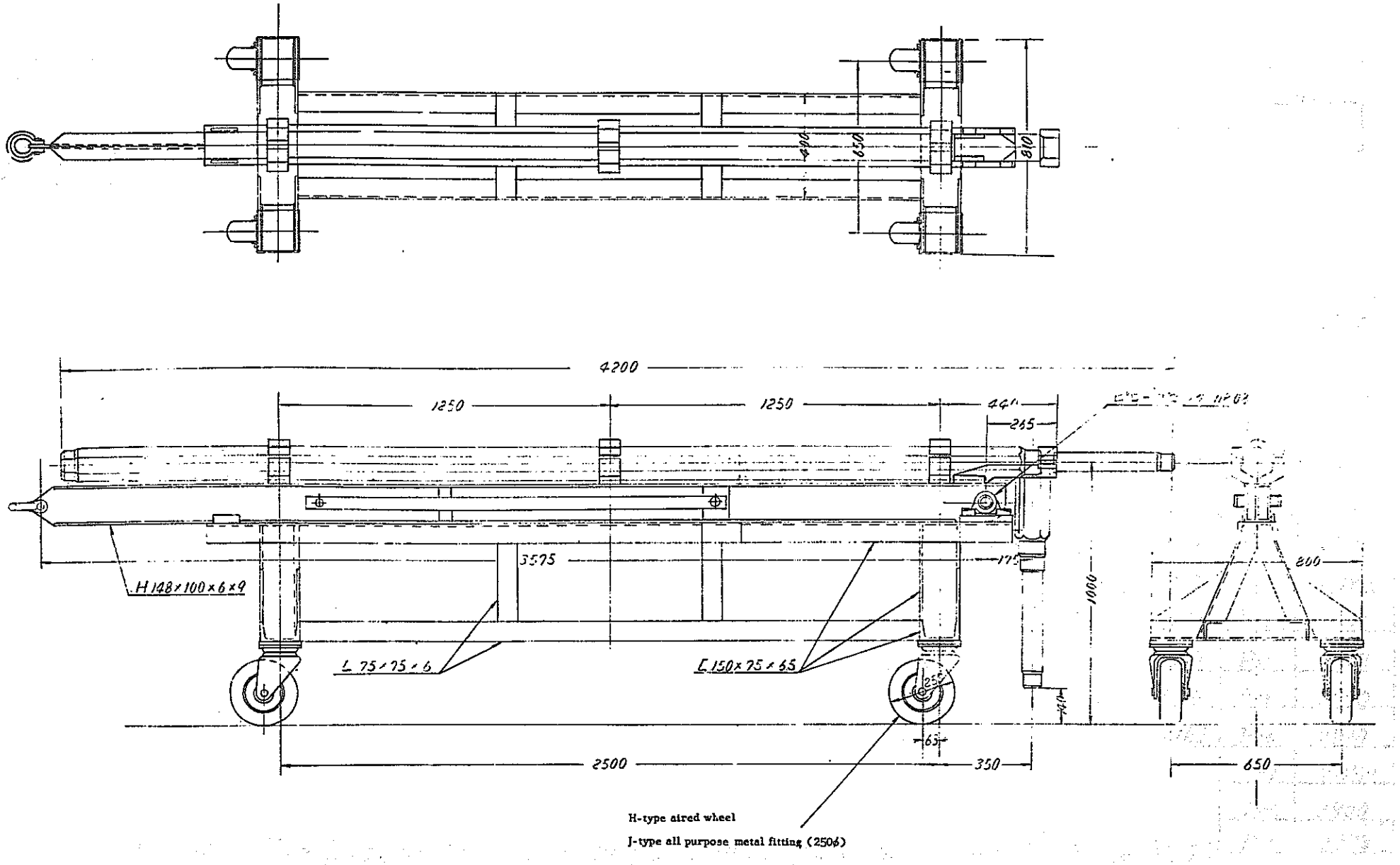

Fig. 5. Tilting Machine

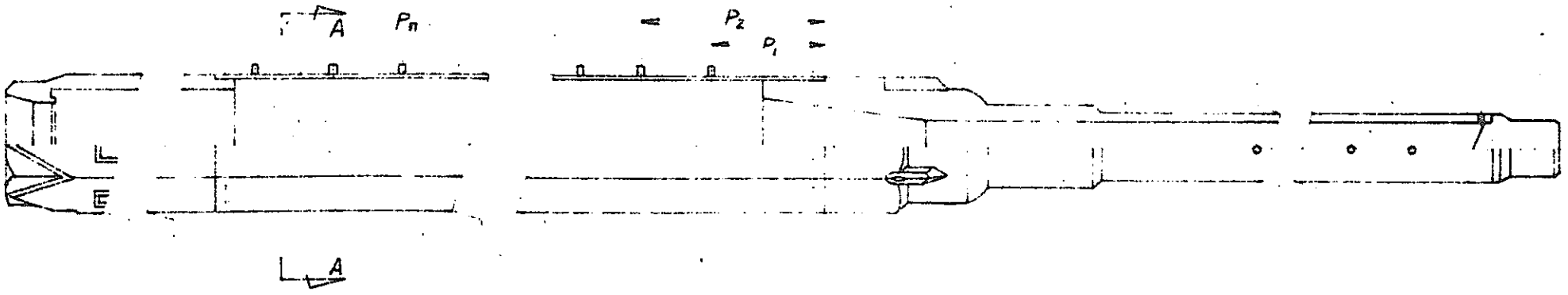

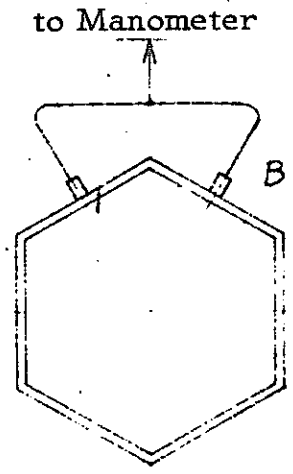

A-A Section

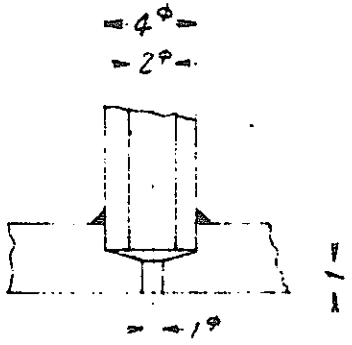

B Details

Tap No.	Place (mm)	Tap No.	Place (mm)	Tap No.	Place (mm)	Tap No.	Place (mm)
P_1	75	P_{12}	850	P_{23}	1500	P_{34}	2250
P_2	200	P_{13}	915	P_{24}	1560	P_{35}	2300
P_3	260	P_{14}	980	P_{25}	1600	P_{36}	2360
P_4	360	P_{15}	1050	P_{26}	1650	P_{37}	2420
P_5	420	P_{16}	1100	P_{27}	1730	P_{38}	2460
P_6	500	P_{17}	1160	P_{28}	1810	P_{39}	2530
P_7	560	P_{18}	1205	P_{29}	1900	P_{40}	2590
P_8	640	P_{19}	1270	P_{30}	2000	P_{41}	2640
P_9	700	P_{20}	1330	P_{31}	2060	P_{42}	2710
P_{10}	750	P_{21}	1390	P_{32}	2100	P_{43}	2770
P_{11}	800	P_{22}	1450	P_{33}	2160	P_{44}	2810
						P_{45}	2850
						P_{46}	2900
						P_{47}	2973

Fig. 6 The location of tap in wrapper tube for measurement of ΔP_{bundle} (NO.1)

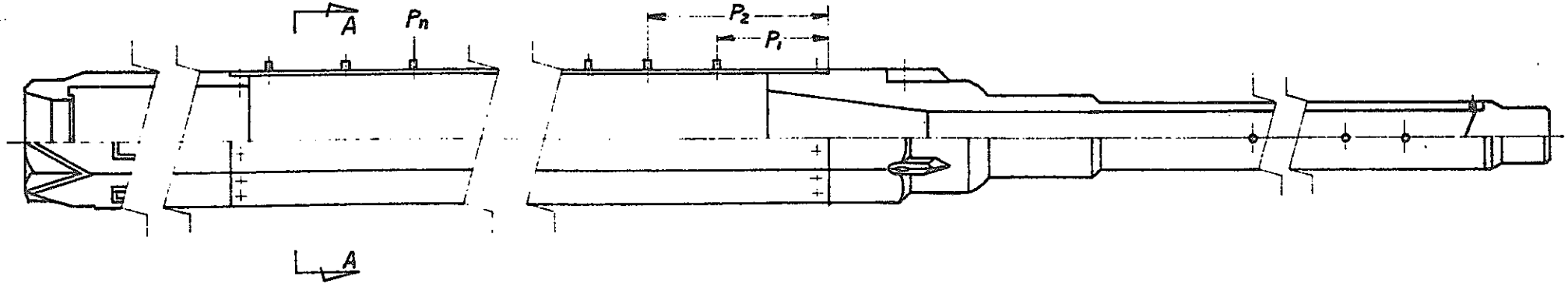

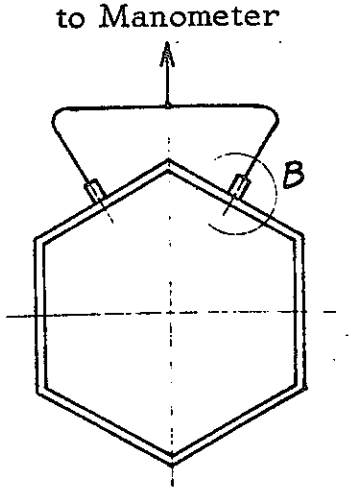

A~A Section

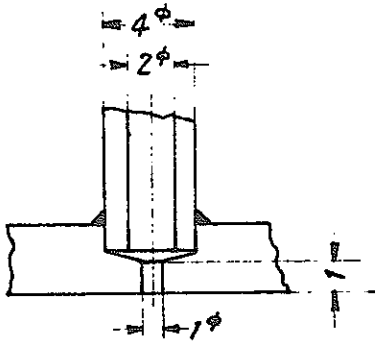

B Details

Tap No.	Place (mm)	Tap No.	Place (mm)	Tap No.	Place (mm)
P_1	63	P_{12}	1155	P_{23}	2222
P_2	168	P_{13}	1222	P_{24}	2355
P_3	228	P_{14}	1355	P_{25}	2422
P_4	355	P_{15}	1422	P_{26}	2555
P_5	422	P_{16}	1555	P_{27}	2622
P_6	555	P_{17}	1622	P_{28}	2755
P_7	622	P_{18}	1755	P_{29}	2822
P_8	755	P_{19}	1822	P_{30}	2923
P_9	822	P_{20}	1955	P_{31}	2958
P_{10}	955	P_{21}	2022	P_{32}	2973
P_{11}	1022	P_{22}	2155	P_{33}	

Fig. 7 The location of tap in wrapper tube for measurement of ΔP_{Bundle} (NO. 2)

Fig. 8 The location of taps for pressure measurement (NFI (Sumitomo) grid)

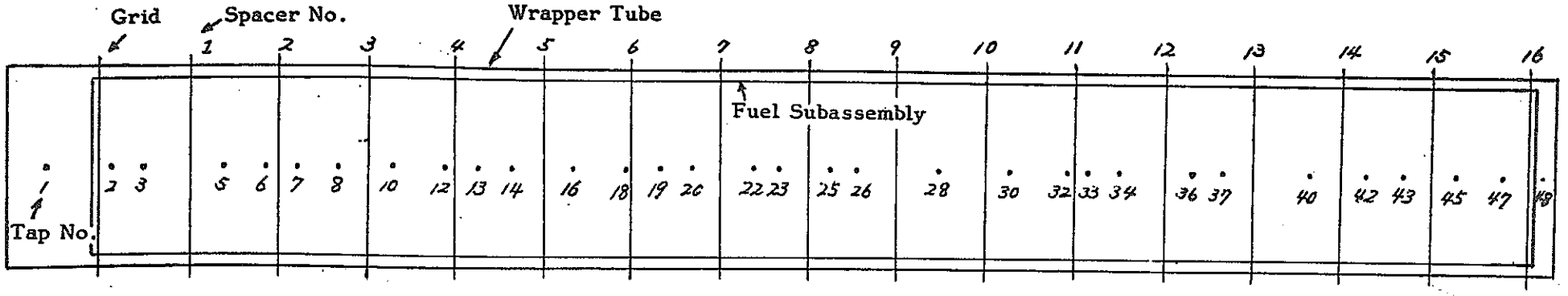

Tap No.	Place of Tap	Place of Spacer	Tap No.	Place of Tap	Place of Spacer
1	75 (mm)		23	1500 (mm)	1559 (mm)
2	200		25	1600	
3	260	355 (mm)	26	1650	1731
5	420		28	1810	1903
6	500	527	30	1950	
7	560		32	2060	2075
8	640	699	33	2100	
10	750		34	2160	2247
12	850	871	36	2300	
13	915		37	2360	2449
14	980	1043	40	2530	2591
16	1100		42	2640	2763
18	1205	1215	43	2710	
19	1270		45	2810	
20	1330	1387	47	2900	2952
22	1450		48	2973	

Fig. 9 The location of taps for pressure measurement (Toshiba grid)

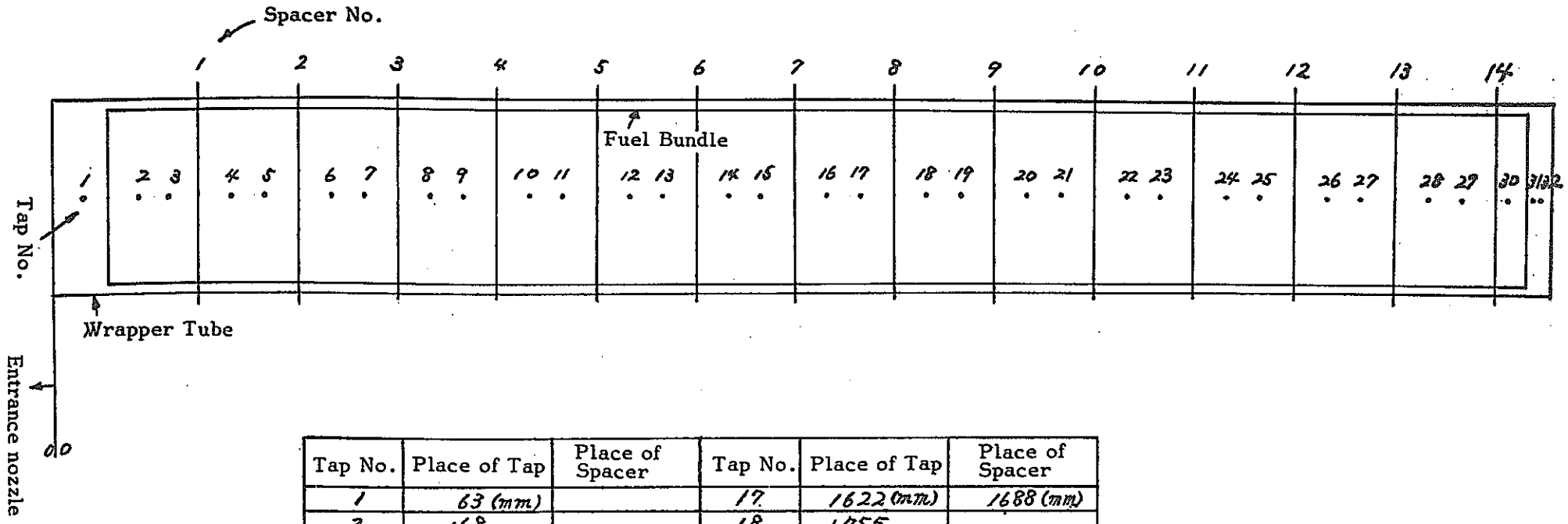

Tap No.	Place of Tap	Place of Spacer	Tap No.	Place of Tap	Place of Spacer
1	63 (mm)		17	1622 (mm)	1688 (mm)
2	168		18	1755	
3	228	288 (mm)	19	1822	1888
4	355		20	1955	
5	422	488	21	2022	2088
6	555		22	2155	
7	622	688	23	2222	2288
8	755		24	2355	
9	822	888	25	2422	2488
10	955		26	2555	
11	1022	1088	27	2622	2688
12	1155		28	2755	
13	1222	1288	29	2822	2888
14	1355		30	2923	
15	1422	1488	31	2958	
16	1555		32	2973	

Fig. 10 The location of taps for pressure measurement (NFI (Furukawa) grid)

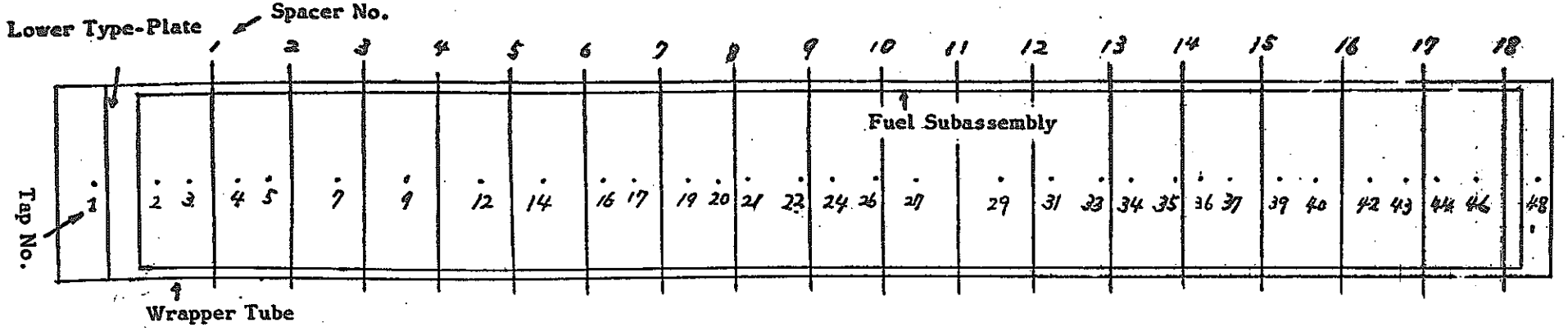

Tap No.	Place of Tap	Place of Spacer	Tap No.	Place of Tap	Place of Spacer
1	75		35	2250	2264.5
2	200		36	2300	
3	260	314.5	37	2360	2424.5
4	360		39	2460	
5	420	464.5	40	2530	2884.5
7	560	614.5	42	2640	
9	700	764.5	43	2910	2744.5
12	850		44	2770	
14	980	914.5	46	2850	2904.5
16	1100	1064.5	48	2973	
17	1160	1214.5			
19	1270				
20	1330	1364.5			
21	1390				
23	1500	1514.5			
24	1560				
26	1650	1664.5			
27	1730				
29	1900	1814.5			
31	2000	1964.5			
33	2100	2114.5			
34	2160				

Fig. 11 The location of taps for pressure measurement (Mitubishi grid)

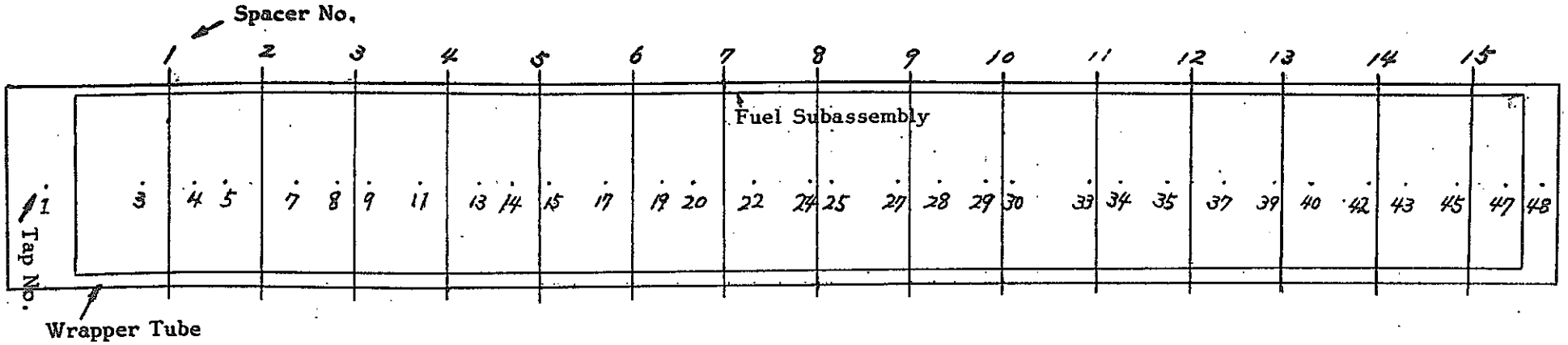

Tap No.	Place of Tap	Place of Spacer	Tap No.	Place of Tap	Place of Spacer
1	75 (mm)		25	1600 (mm)	
3	260	315 (mm)	27	1730	1755 (mm)
4	360		28	1810	
5	420	495	29	1900	1935
7	560		30	1950	
8	640	675	33	2100	2115
9	700		34	2160	
11	800	855	35	2250	2295
13	915		37	2360	
14	980		39	2460	2475
15	1050	1035	40	2530	
17	1160	1215	42	2640	2655
19	1270		43	2710	
20	1330	1395	45	2810	2835
22	1450		47	2900	
24	1560	1575	48	2973	

Fig.12 The location of taps for pressure measurement (Hitachi grid)

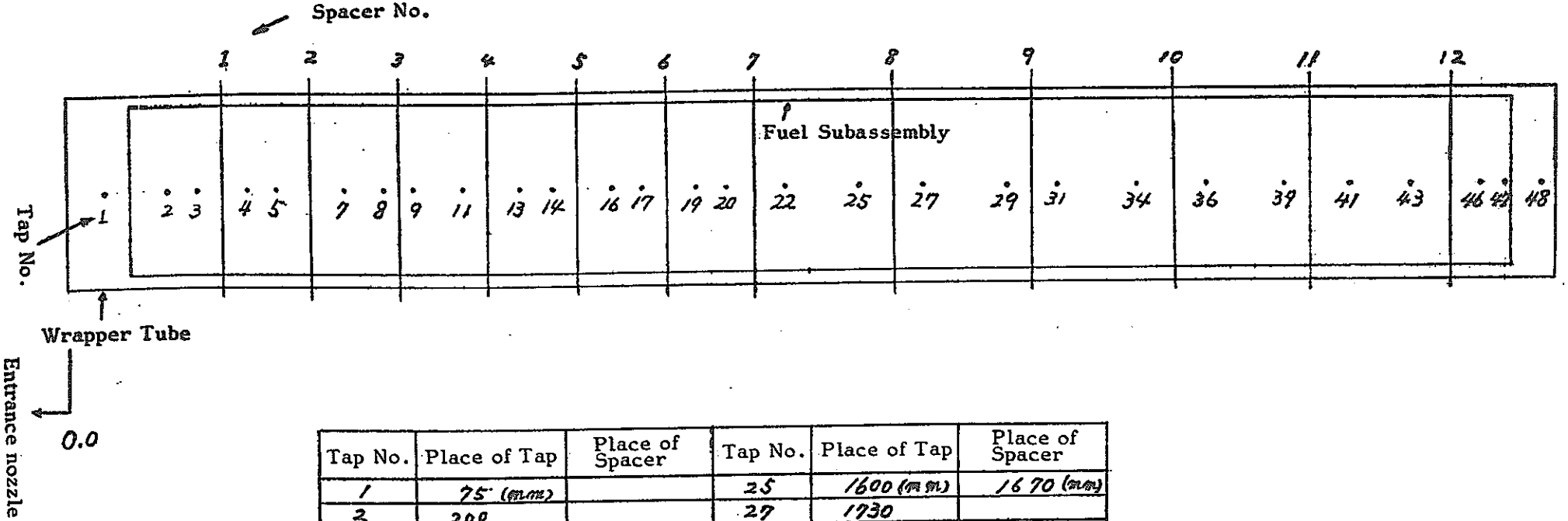

Tap No.	Place of Tap	Place of Spacer	Tap No.	Place of Tap	Place of Spacer
1	75 (mm)		25	1600 (mm)	1670 (mm)
2	200		27	1730	
3	260	310 (mm)	29	1900	1950
4	360		31	2000	
5	420	490	34	2160	2230
7	560		36	2300	
8	640	670	39	2460	2510
9	700		41	2590	
11	800	850	43	2710	2790
13	915		46	2850	
14	980	1030	47	2900	
16	1100		48	2973	
17	1160	1210			
19	1270				
20	1330	1390			
22	1450				

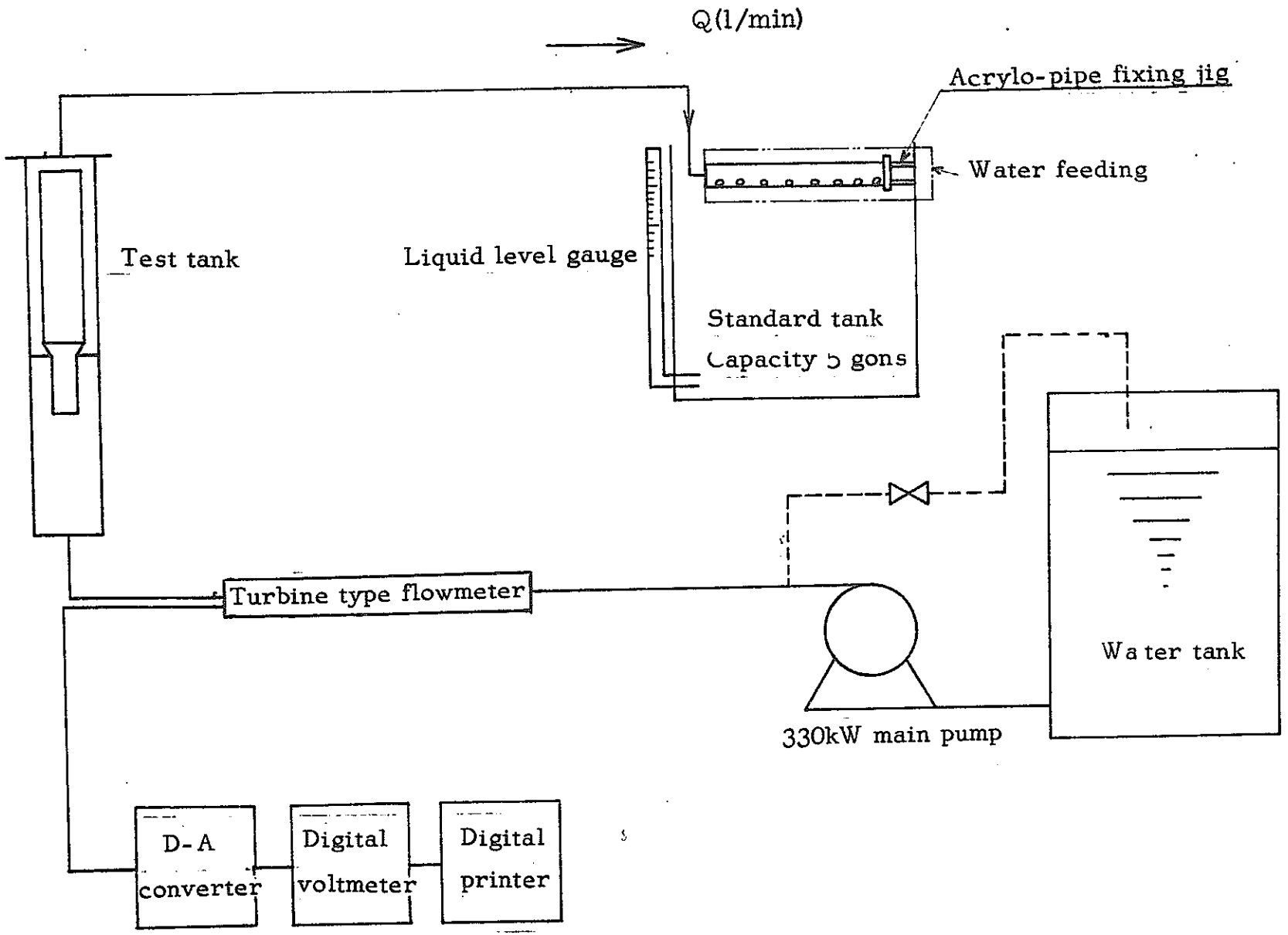

Fig. 13. Block Diagram of Flow Meter Calibration

Fig 14 Flow meter calibration (max. flow rate 240 ton/hr)

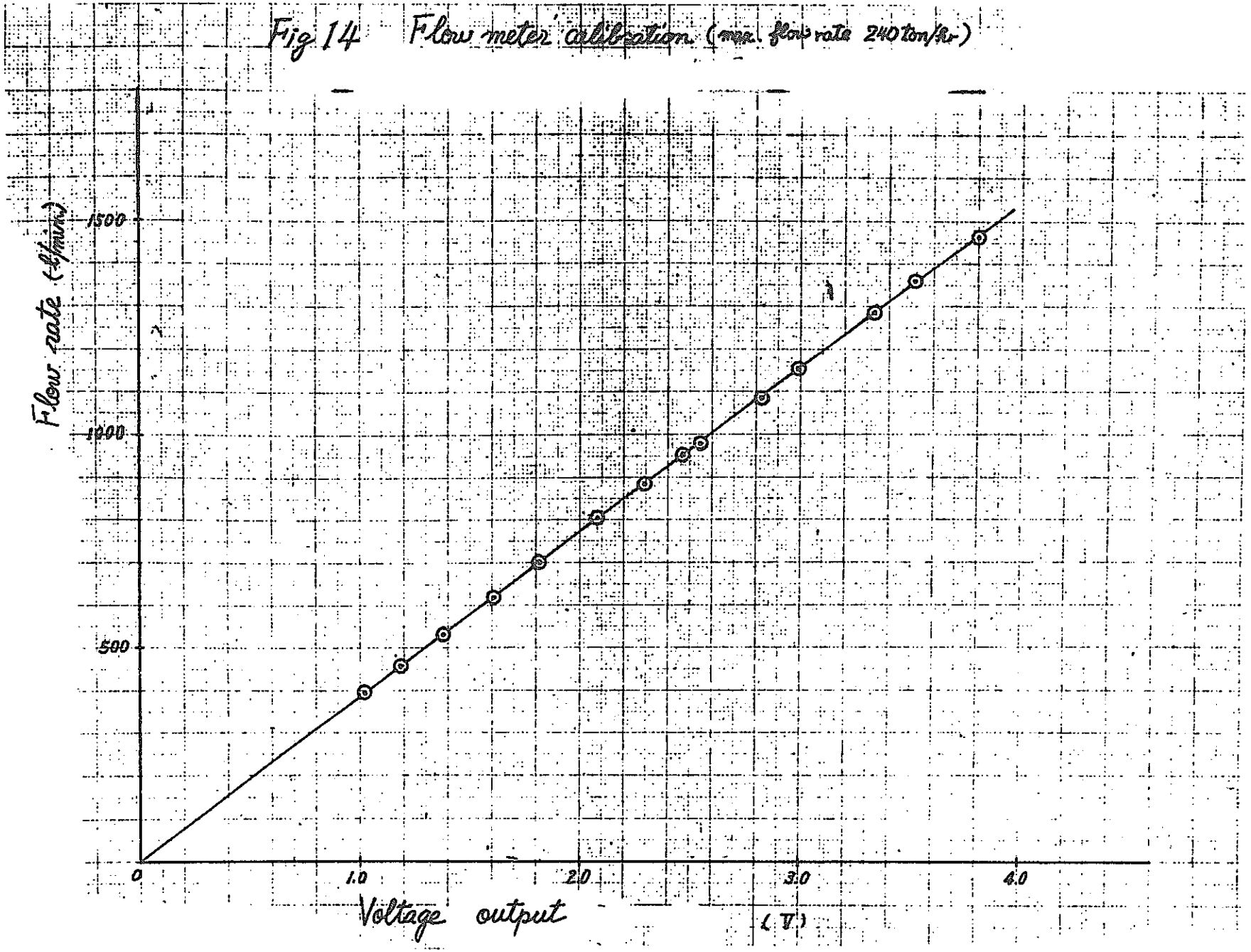

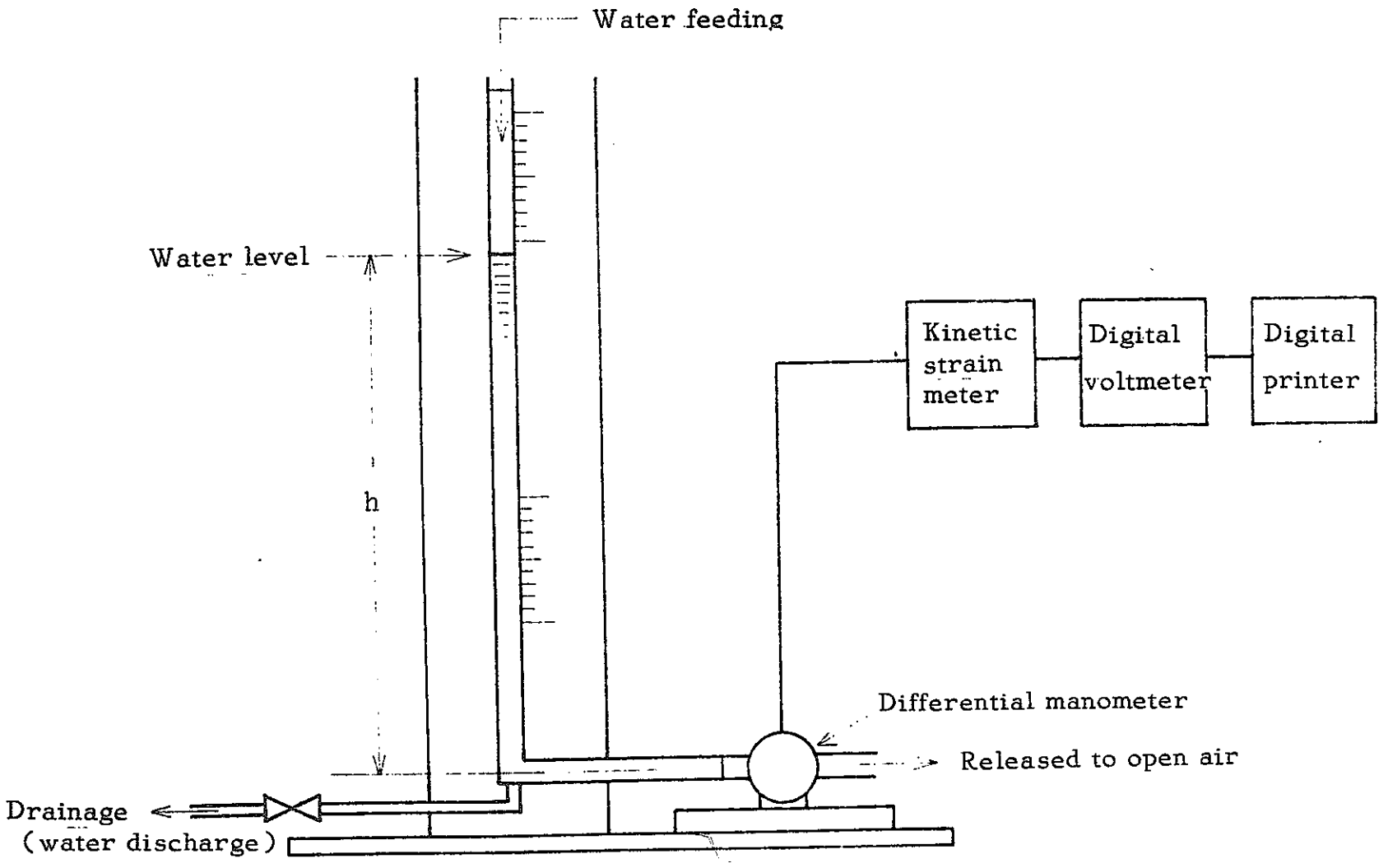

Fig. 15. DP Cell Calibration Device

Fig. 16 DP cell calibration (10 kg/cm²)

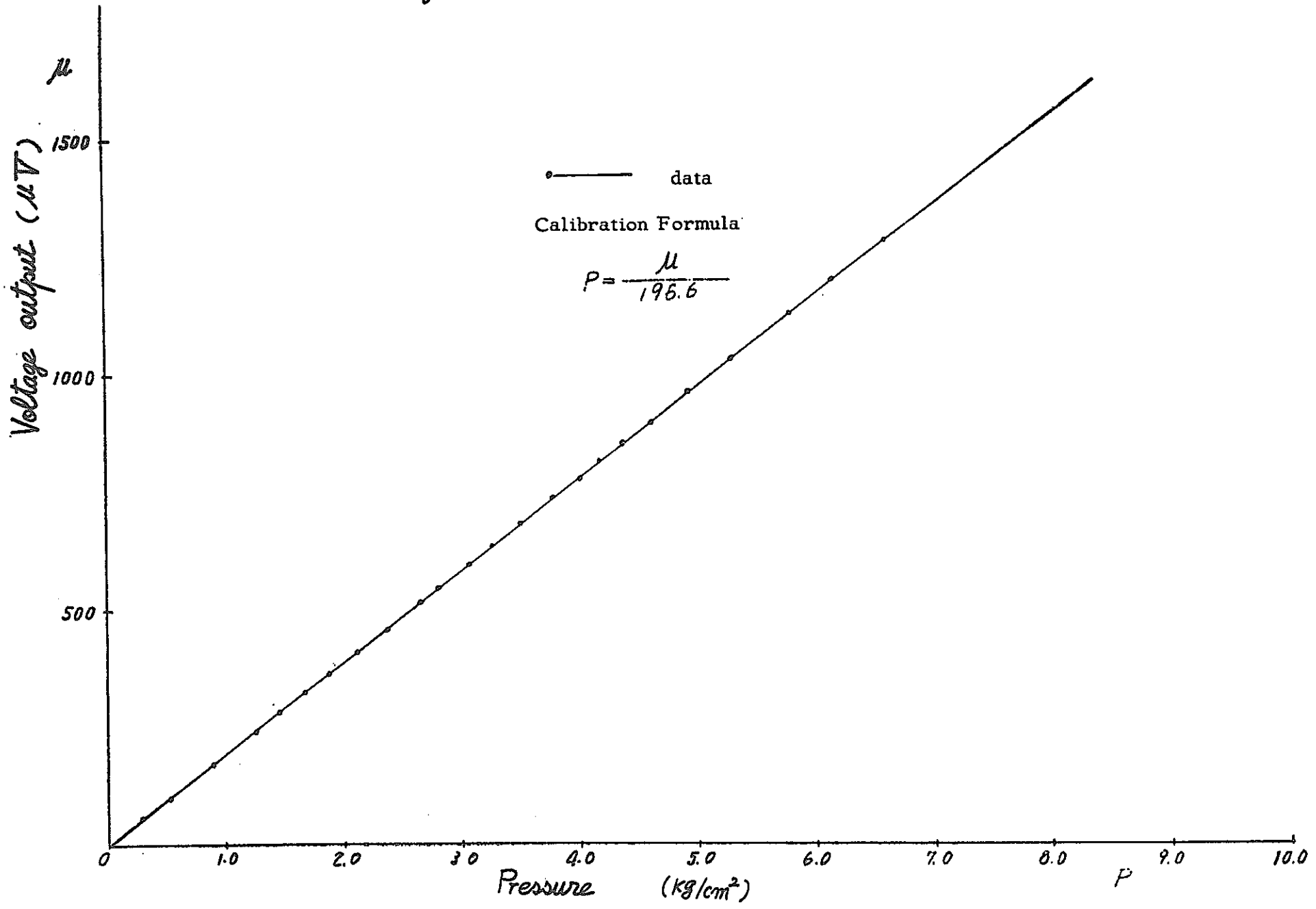

Fig. 17 DP cell calibration (5 kg/cm²)

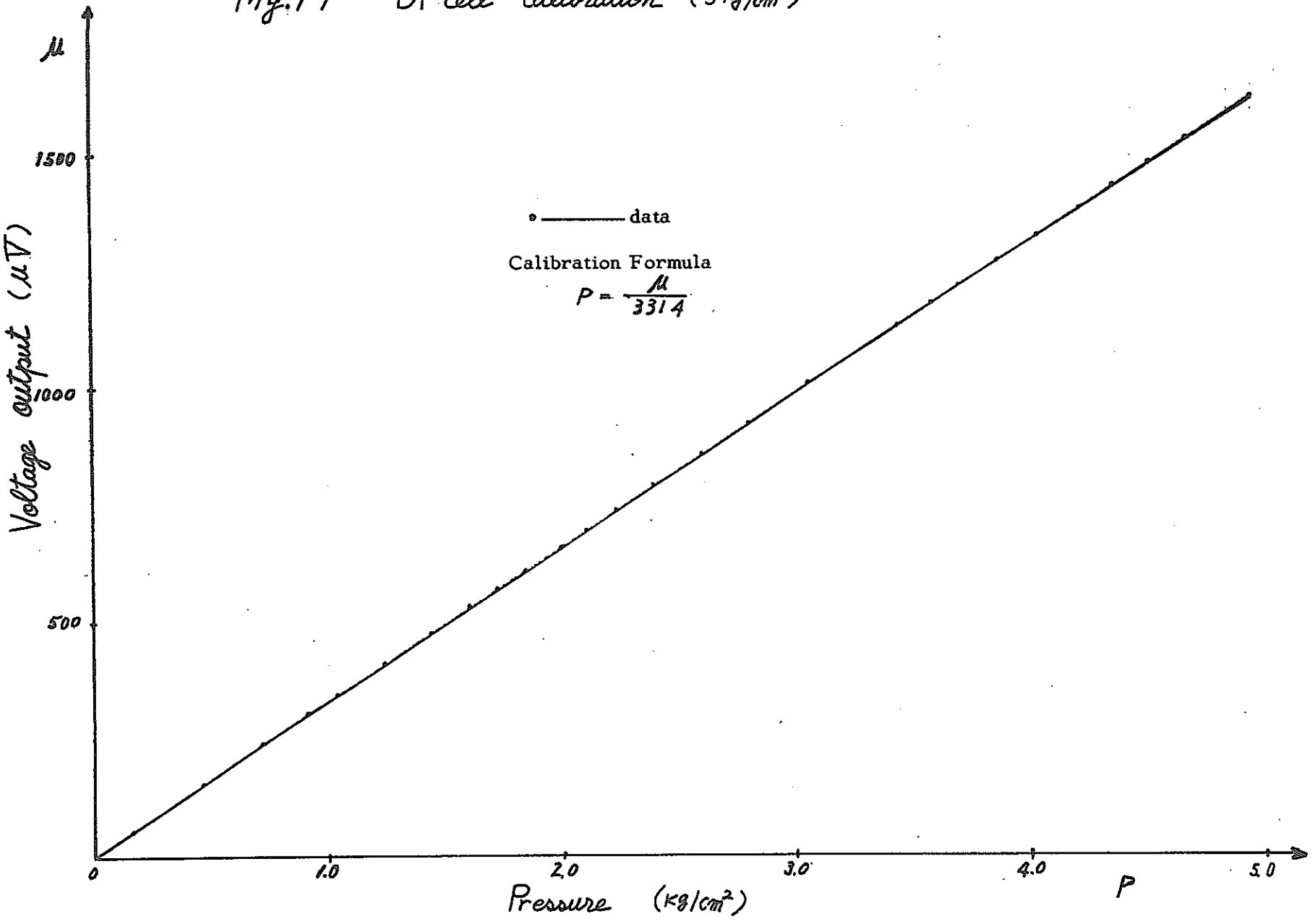

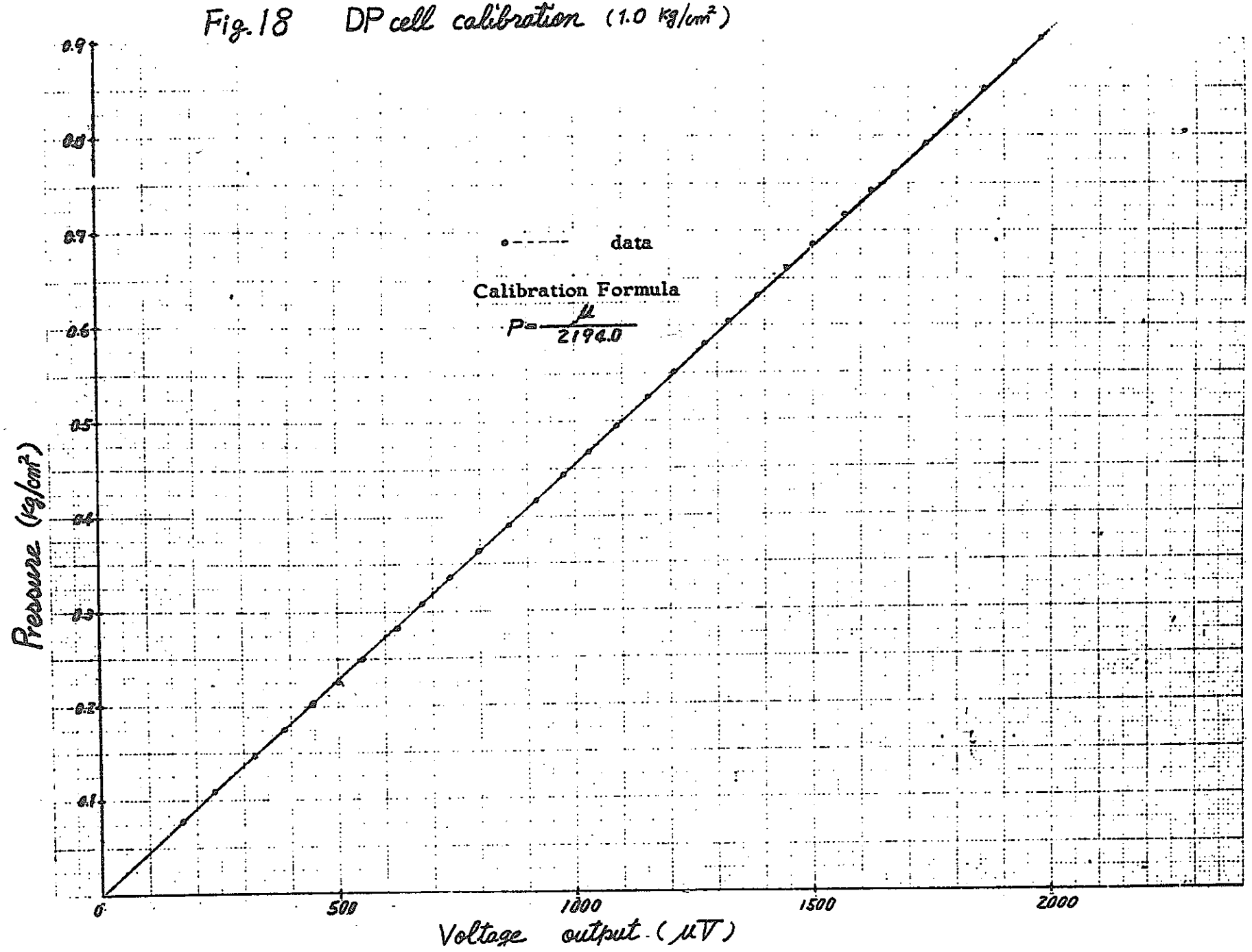
Fig. 18 DP cell calibration (1.0 kg/cm²)
0.9
0.8
0.7
0.6
0.5
0.4
0.3
0.2
0.1
Pressure (kg/cm²)
data
Calibration Formula
P = μ / 2194.0
0
500
1000
1500
2000
Voltage output (μV)

Fig.19 Pressure loss coefficient of fuel assembly (NFI wire type)

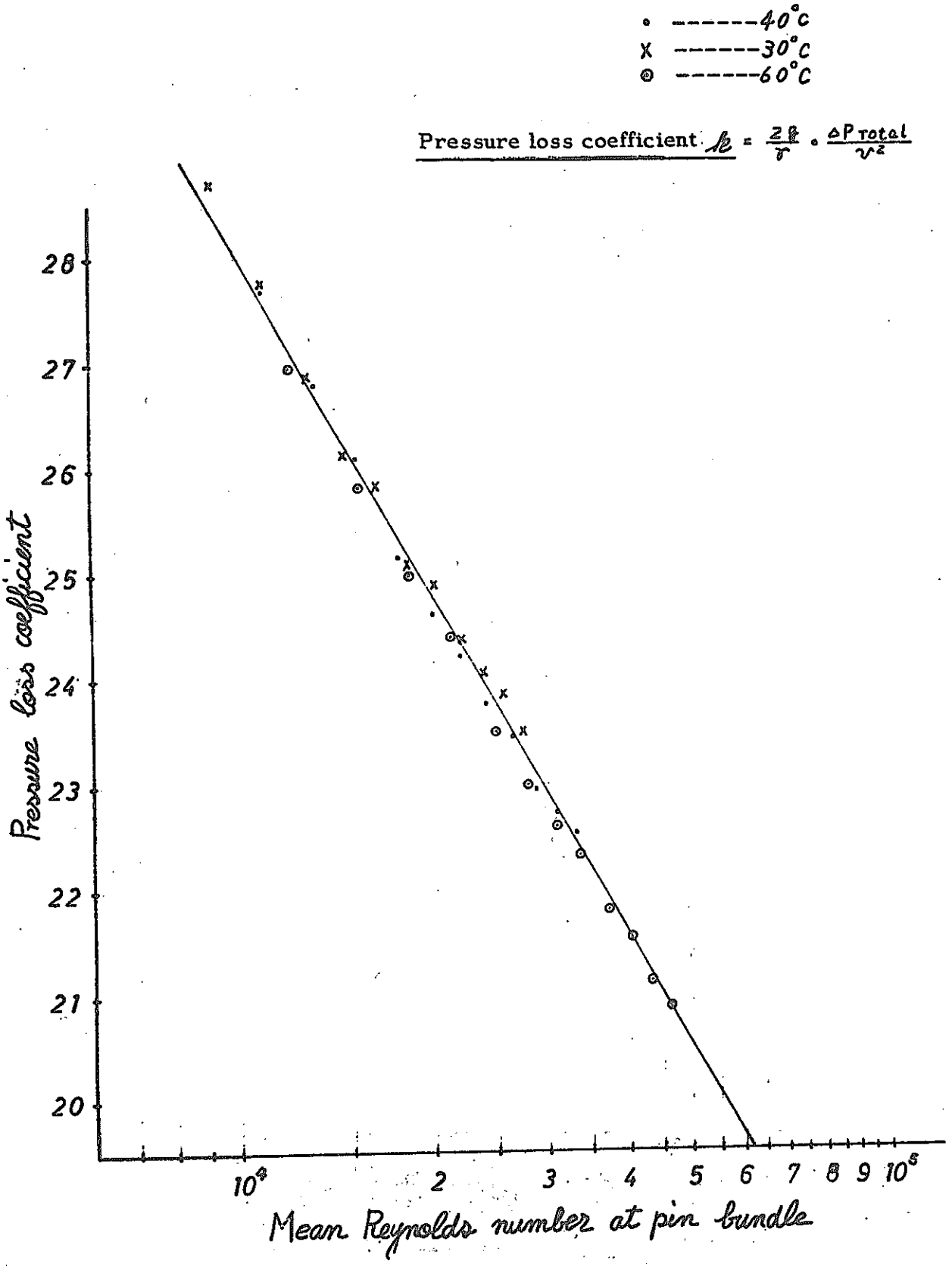

Fig. 20 Total pressure drop in fuel assembly

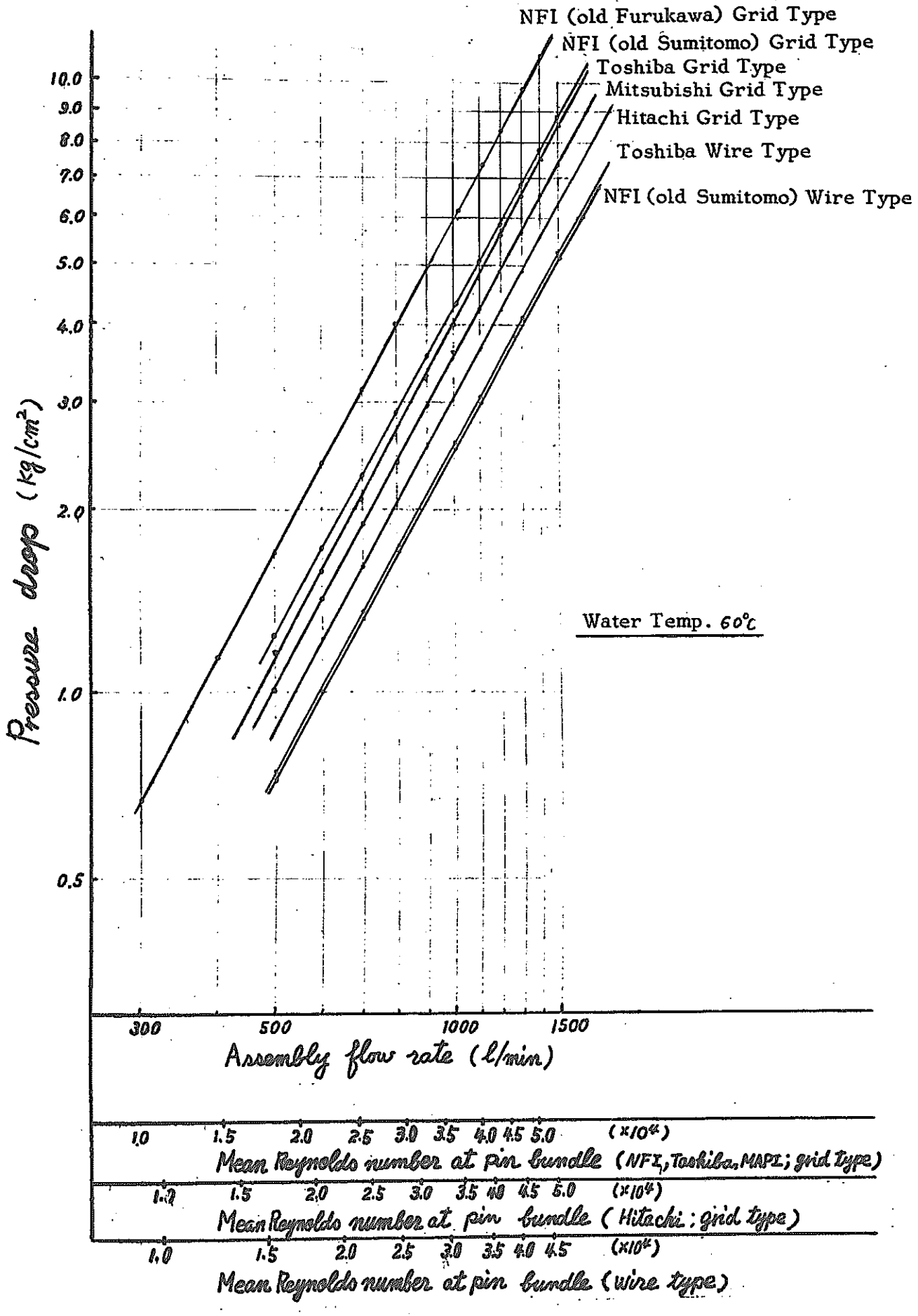

Fig. 21 Pressure loss coefficient of fuel assembly

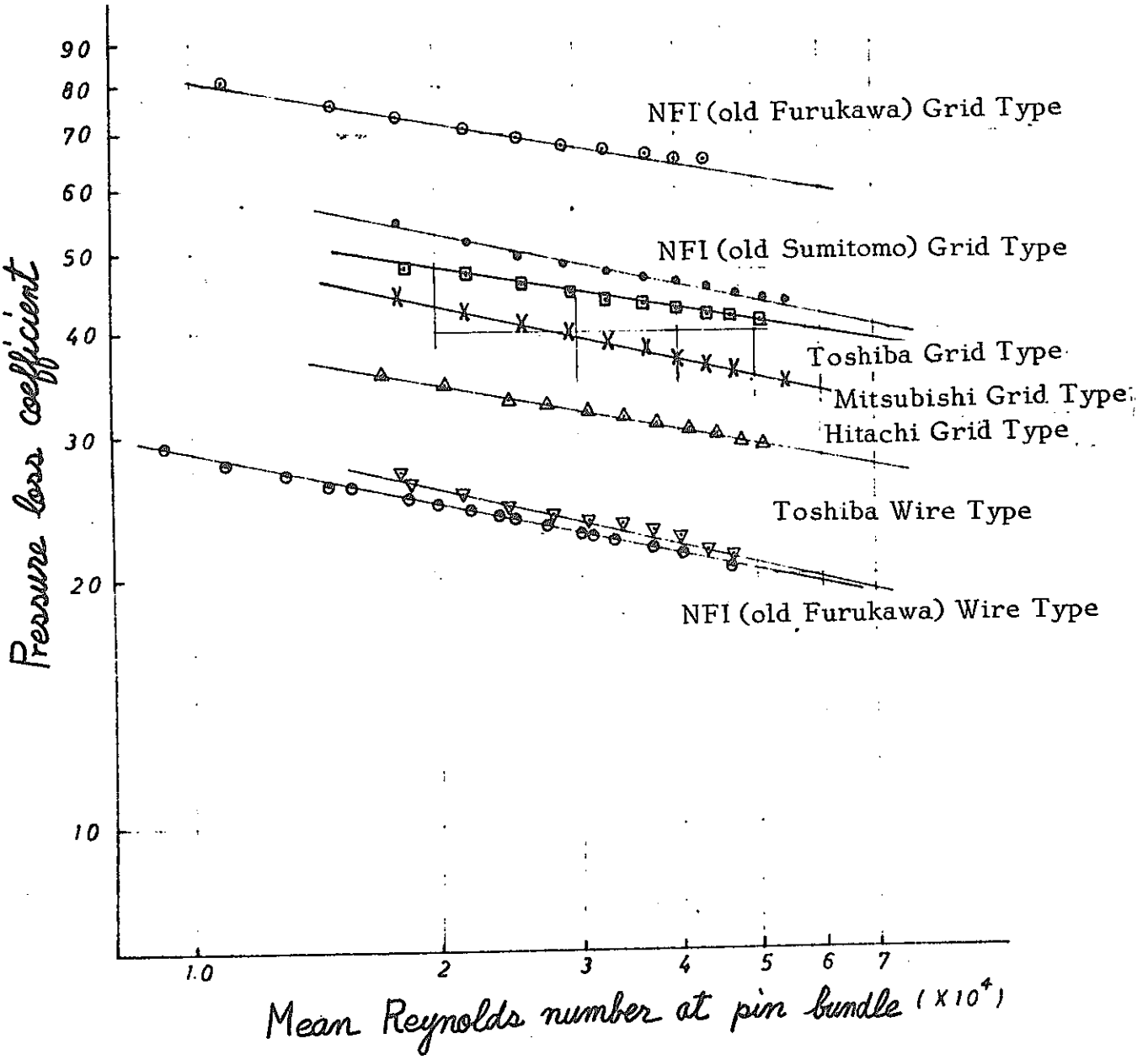

Fig.22 Pressure drop at a spacer (Toshiba grid)

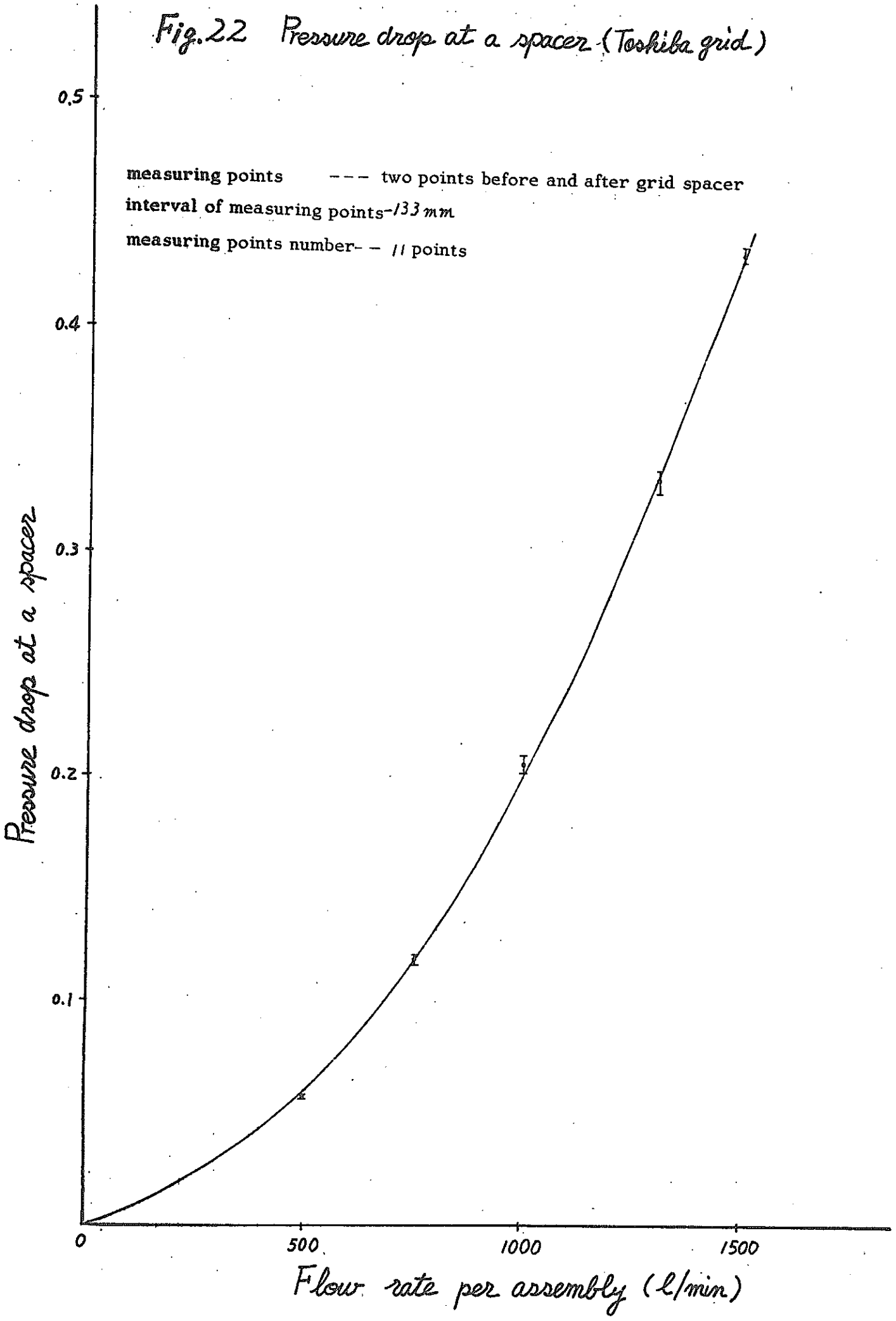

Fig. 23 Pressure drop in pin bundle (Hitachi grid type)

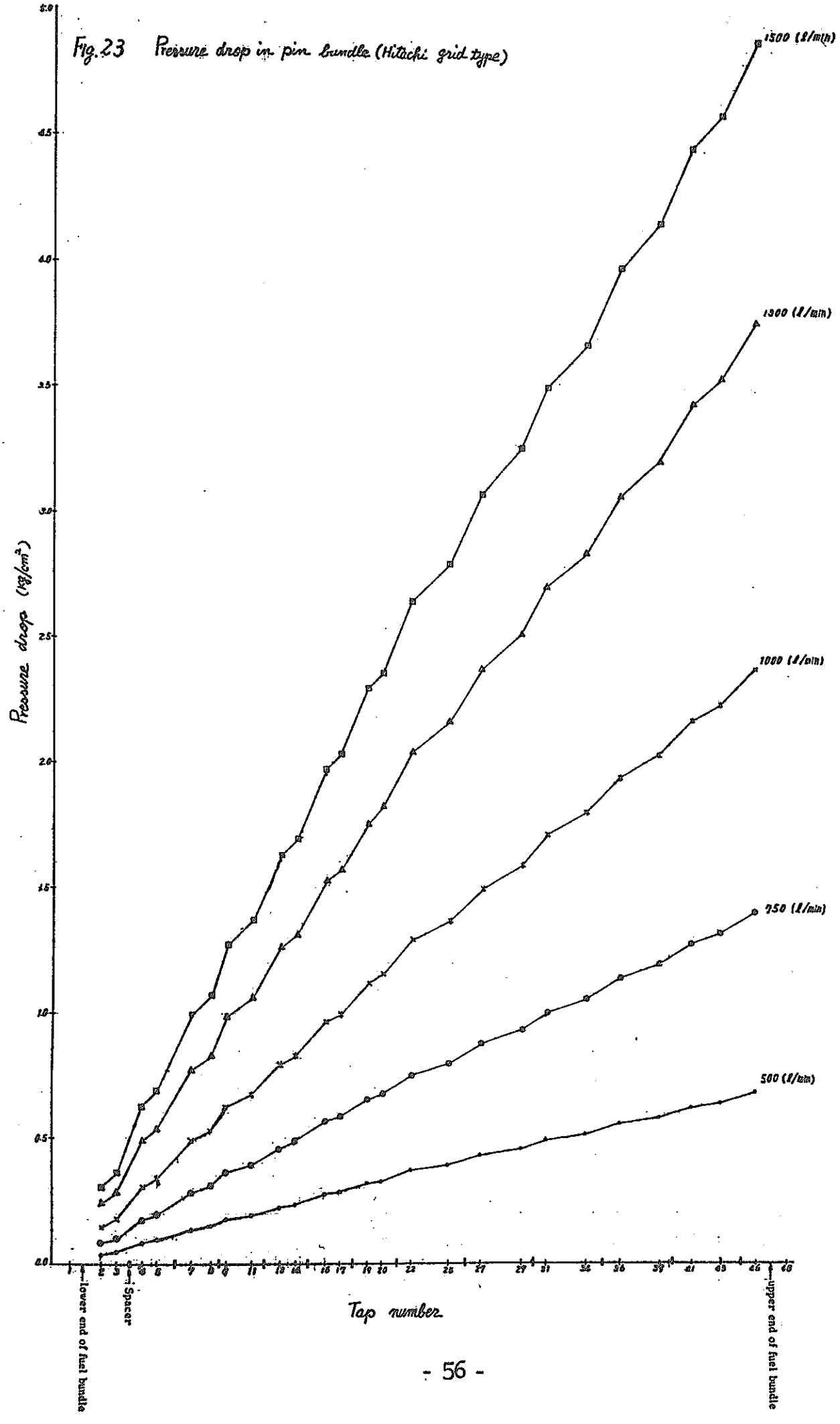

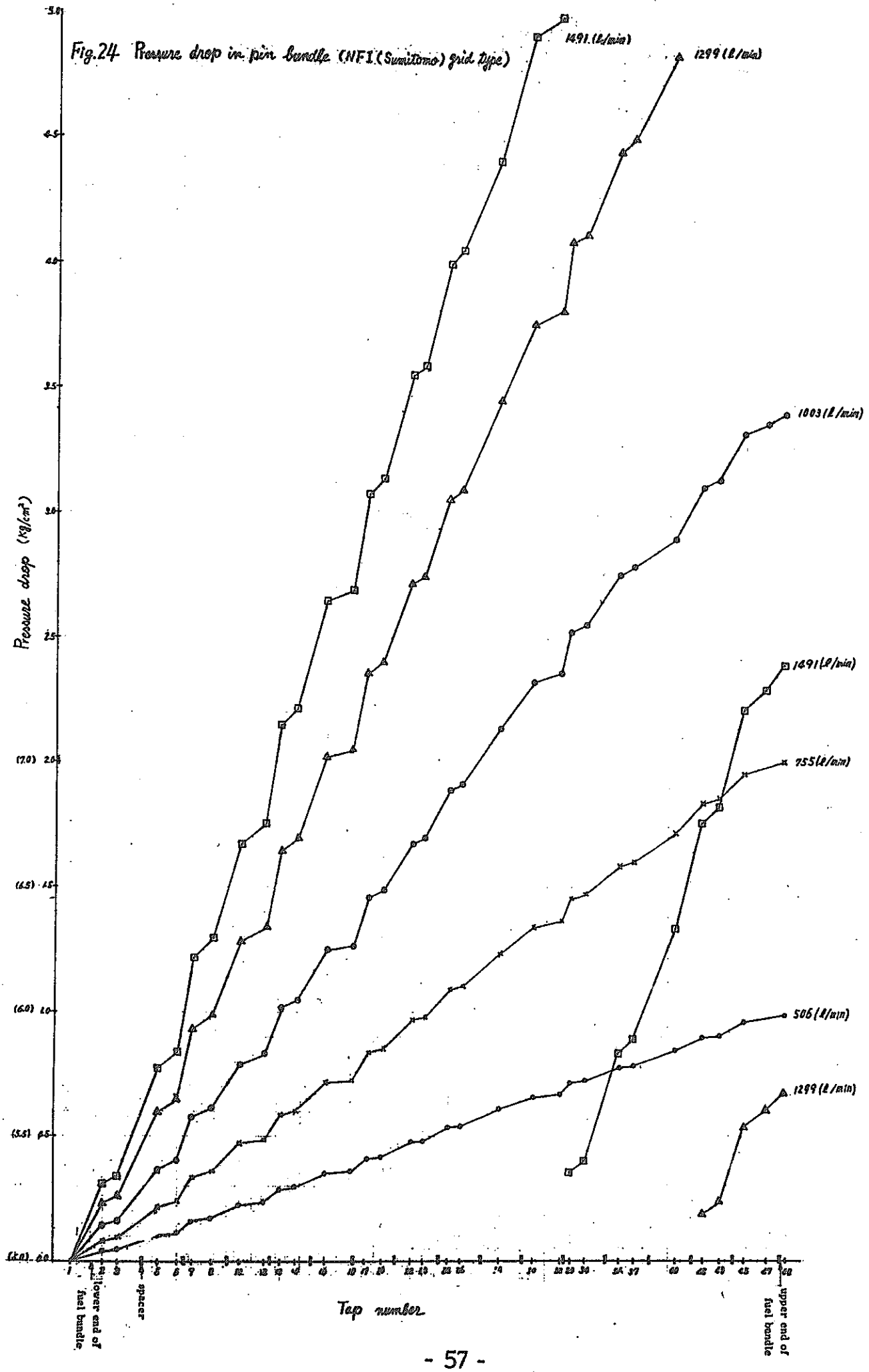
Fig.24 Pressure drop in pin bundle (NFI (Sumitomo) grid type)
1491 (ℓ/min)
1299 (ℓ/min)
1003 (ℓ/min)
1491 (ℓ/min)
755 (ℓ/min)
506 (ℓ/min)
1299 (ℓ/min)
Pressure drop (kg/cm²)
Tap number
lower end of fuel bundle
spacer
upper end of fuel bundle

Fig. 25 Pressure drop in pin bundle (NFI (Furukawa) grid type)

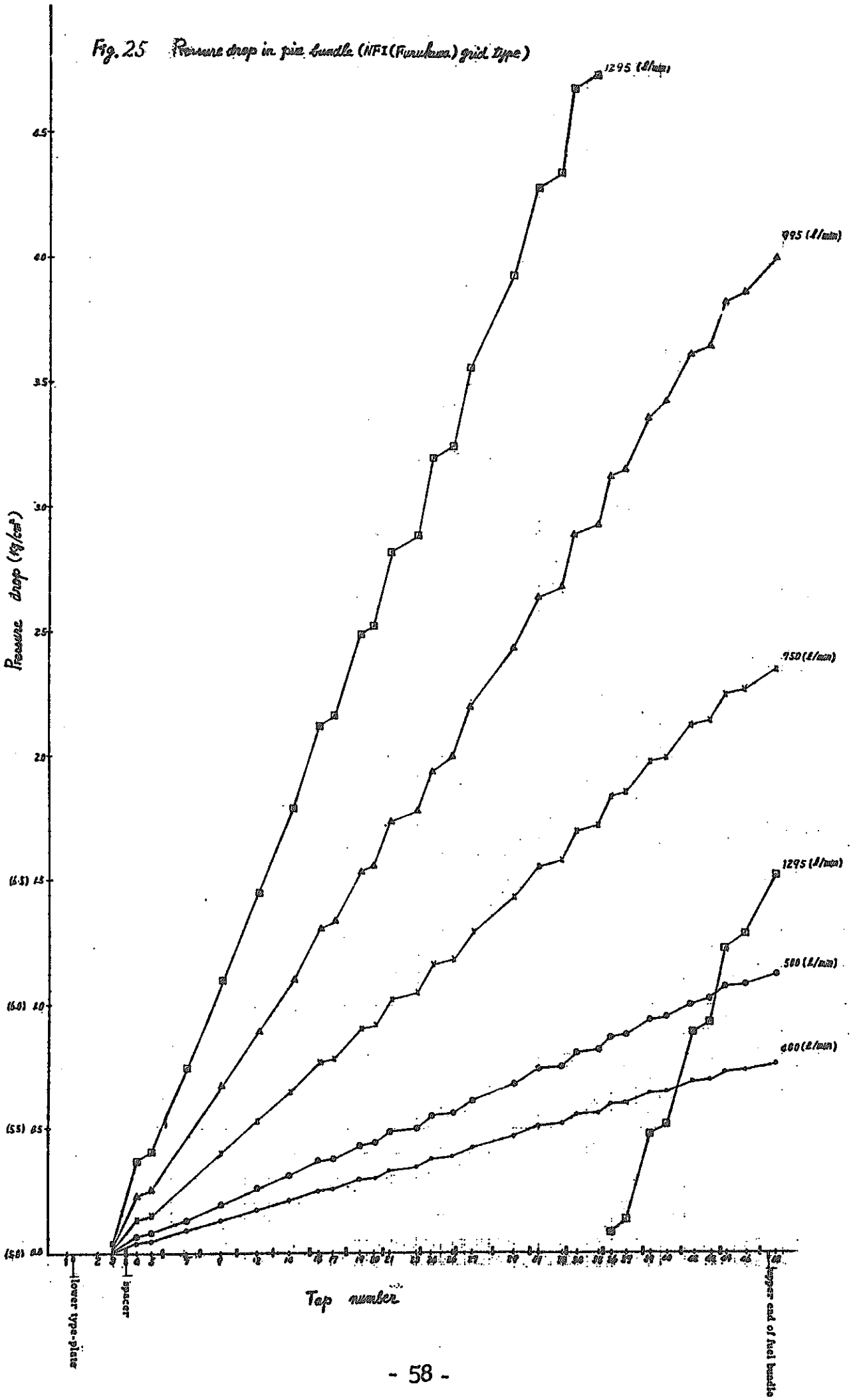

Fig. 26 Pressure drop in pin bundle (Mitubishi grid type)

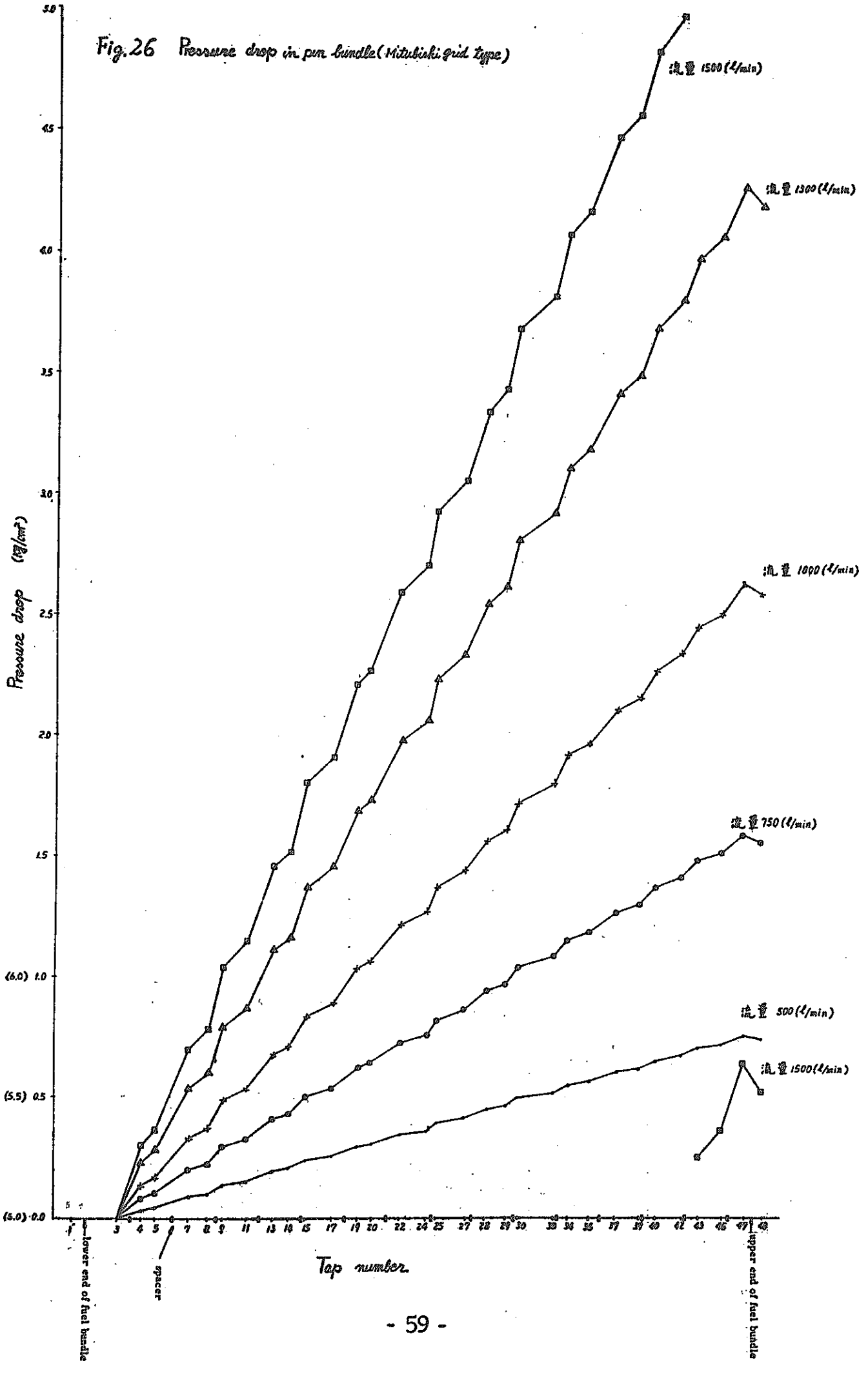

Fig. 27 Spacer loss coefficient

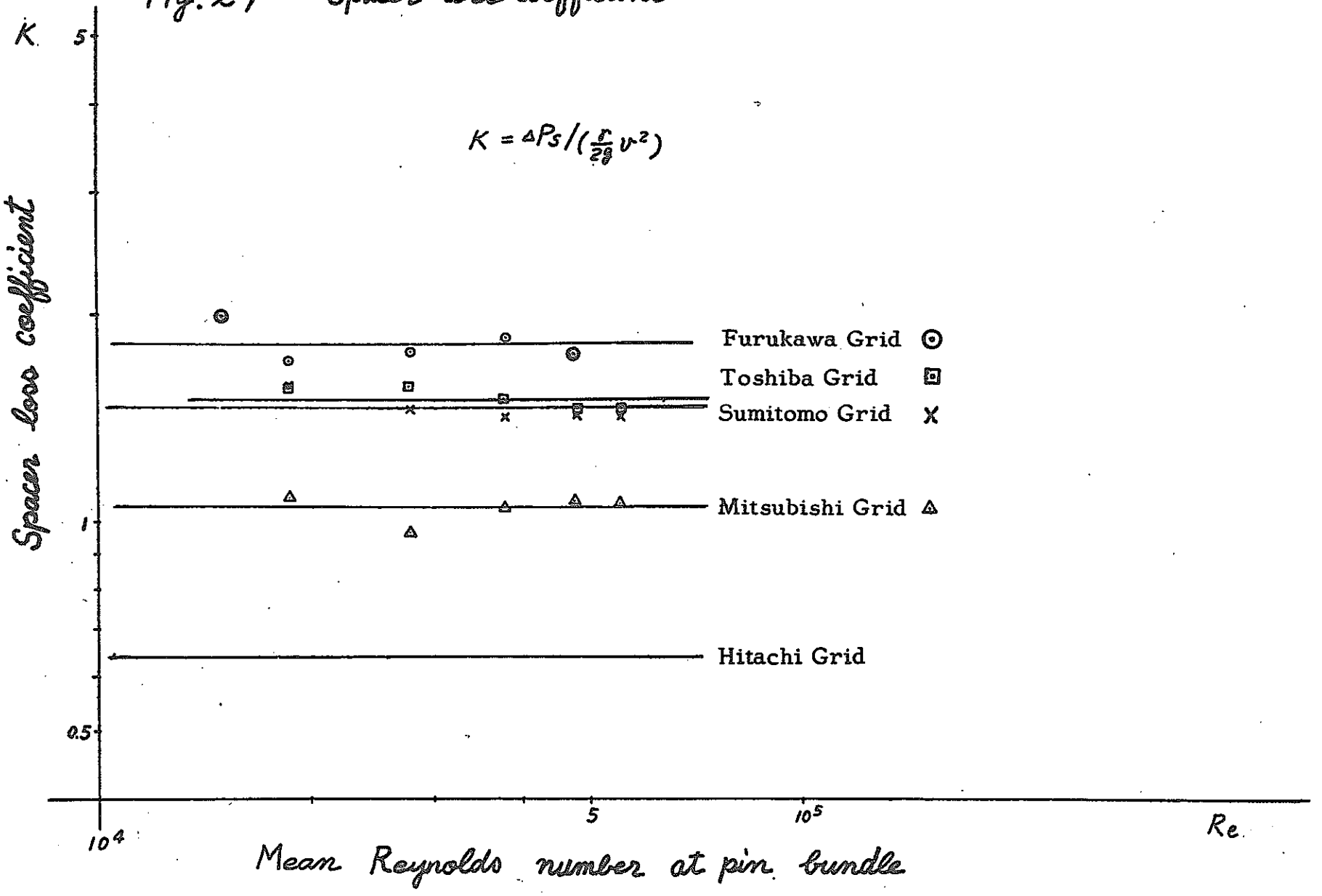

Fig. 28 Friction loss coefficient

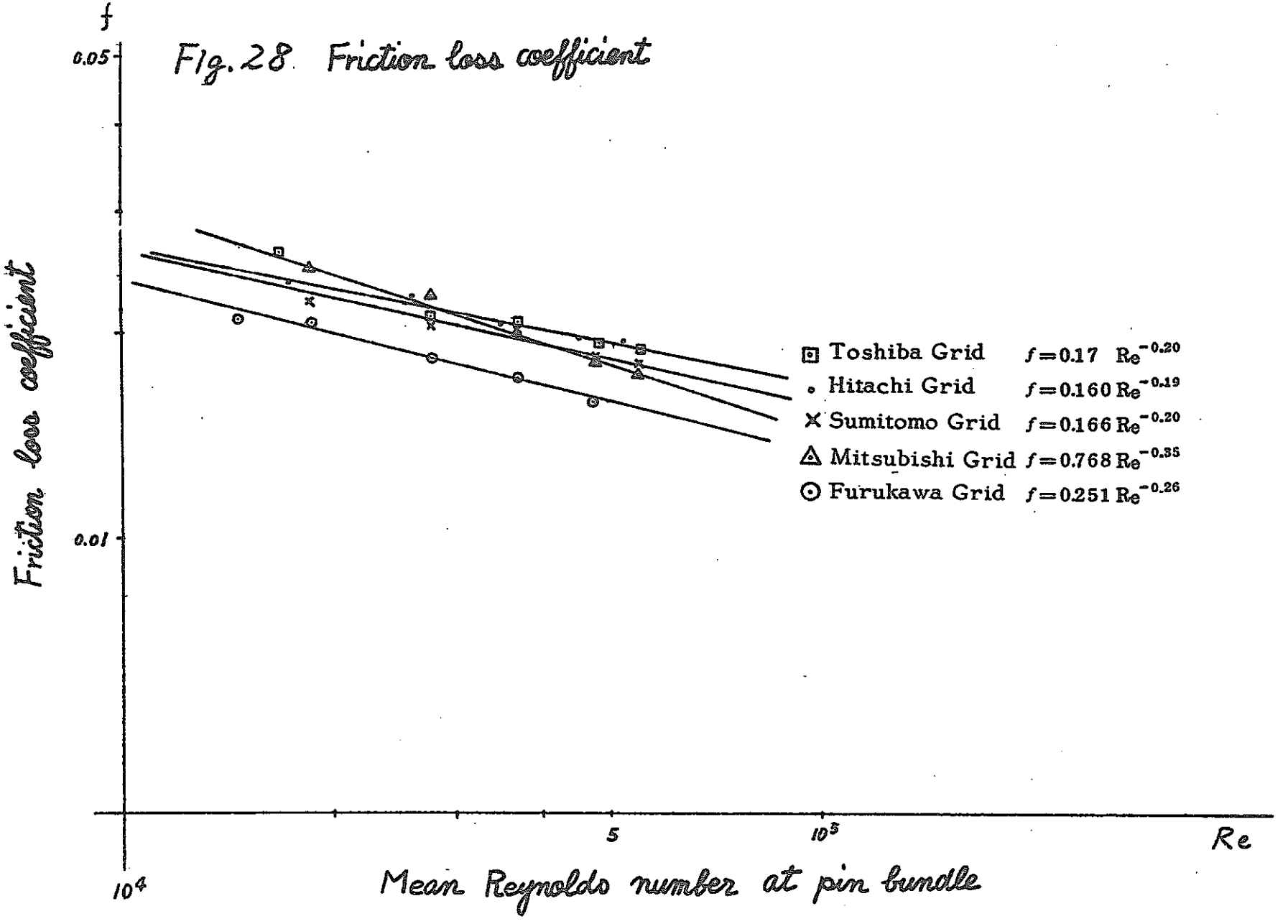

Fig. 29 Total pressure drop in pin bundle (Grid type)

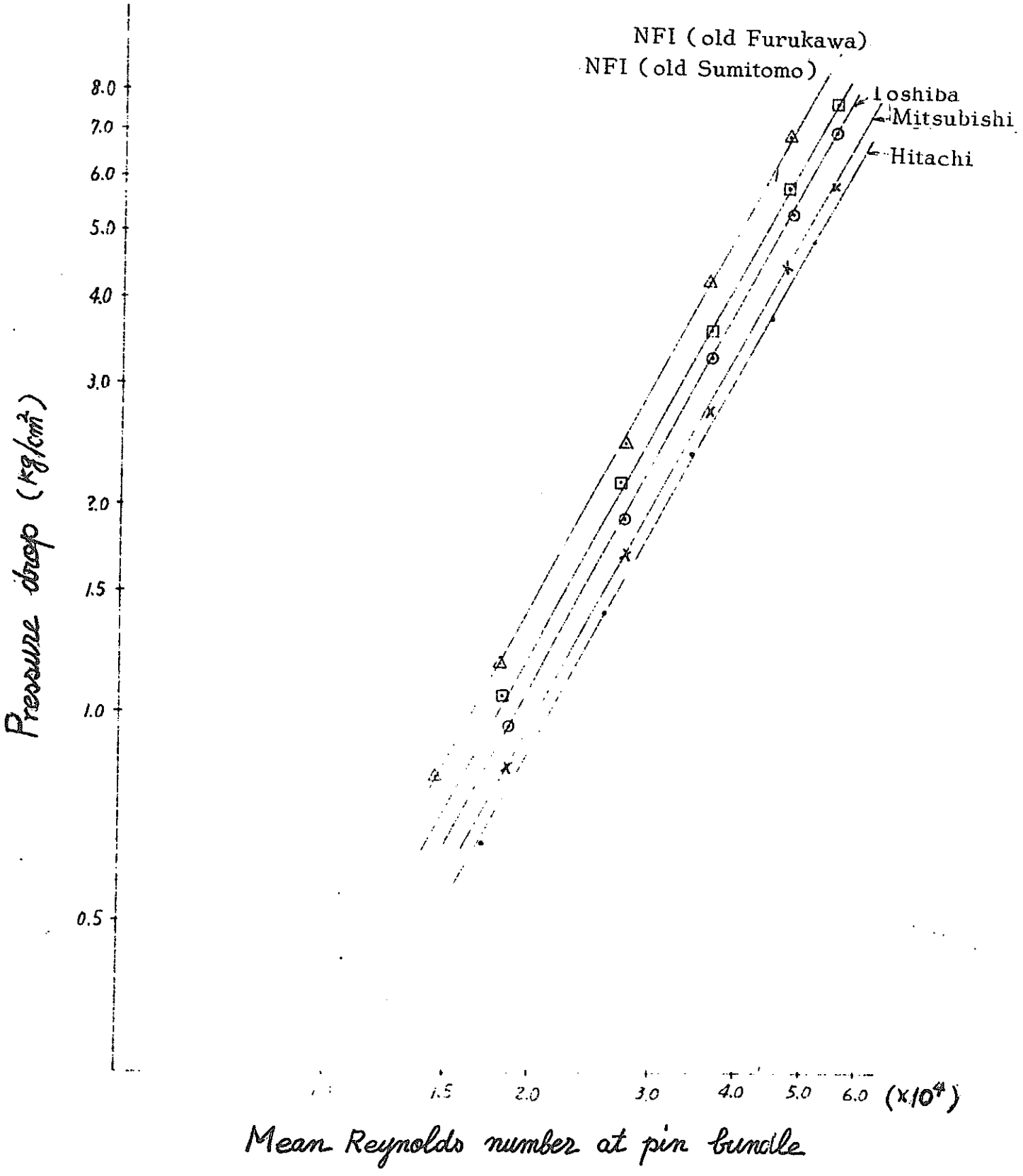

Fig. 30 Pressure drop at pin bundle support

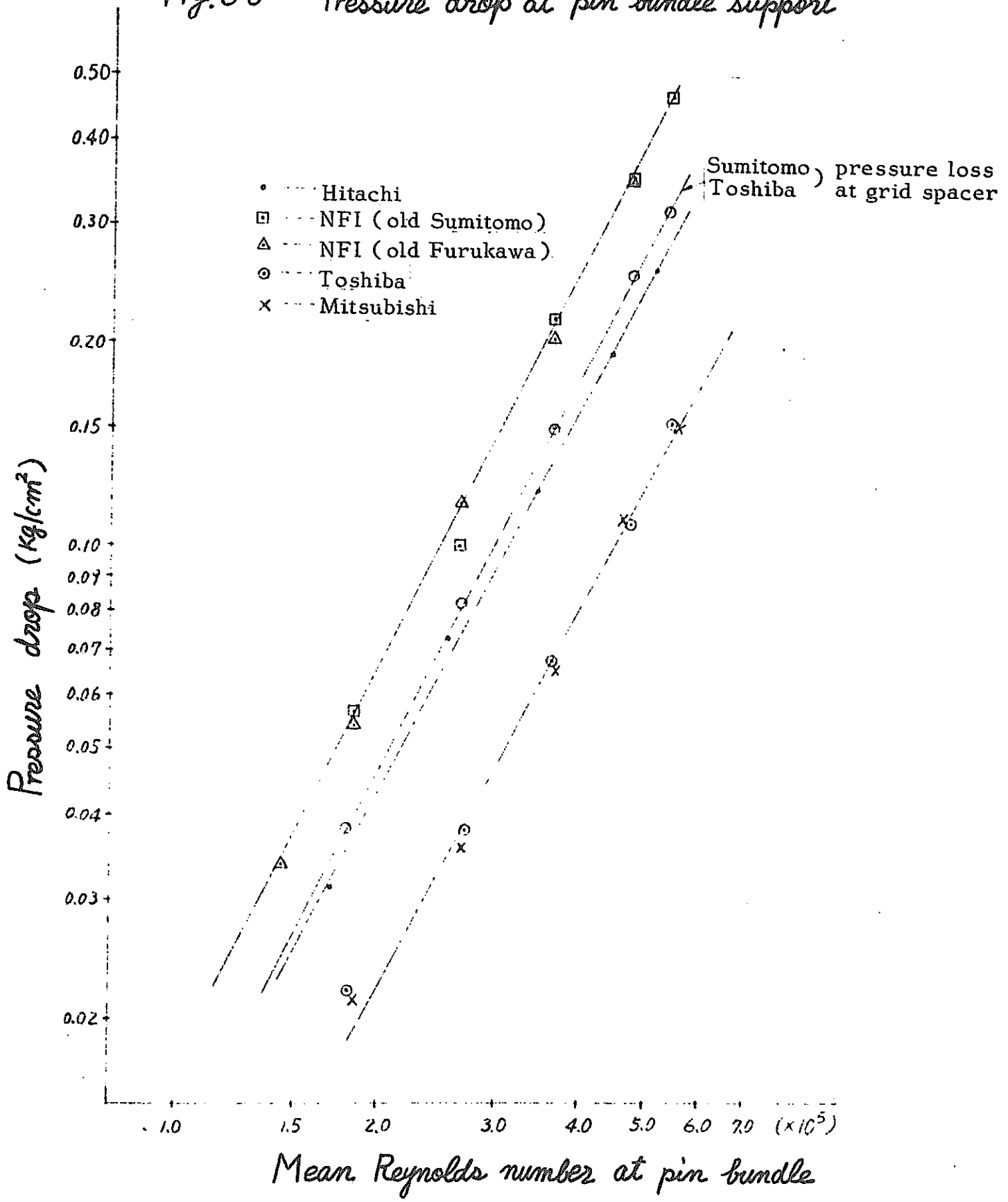

Fig.31 Pressure drop in pin bundle (Toshiba wire type)

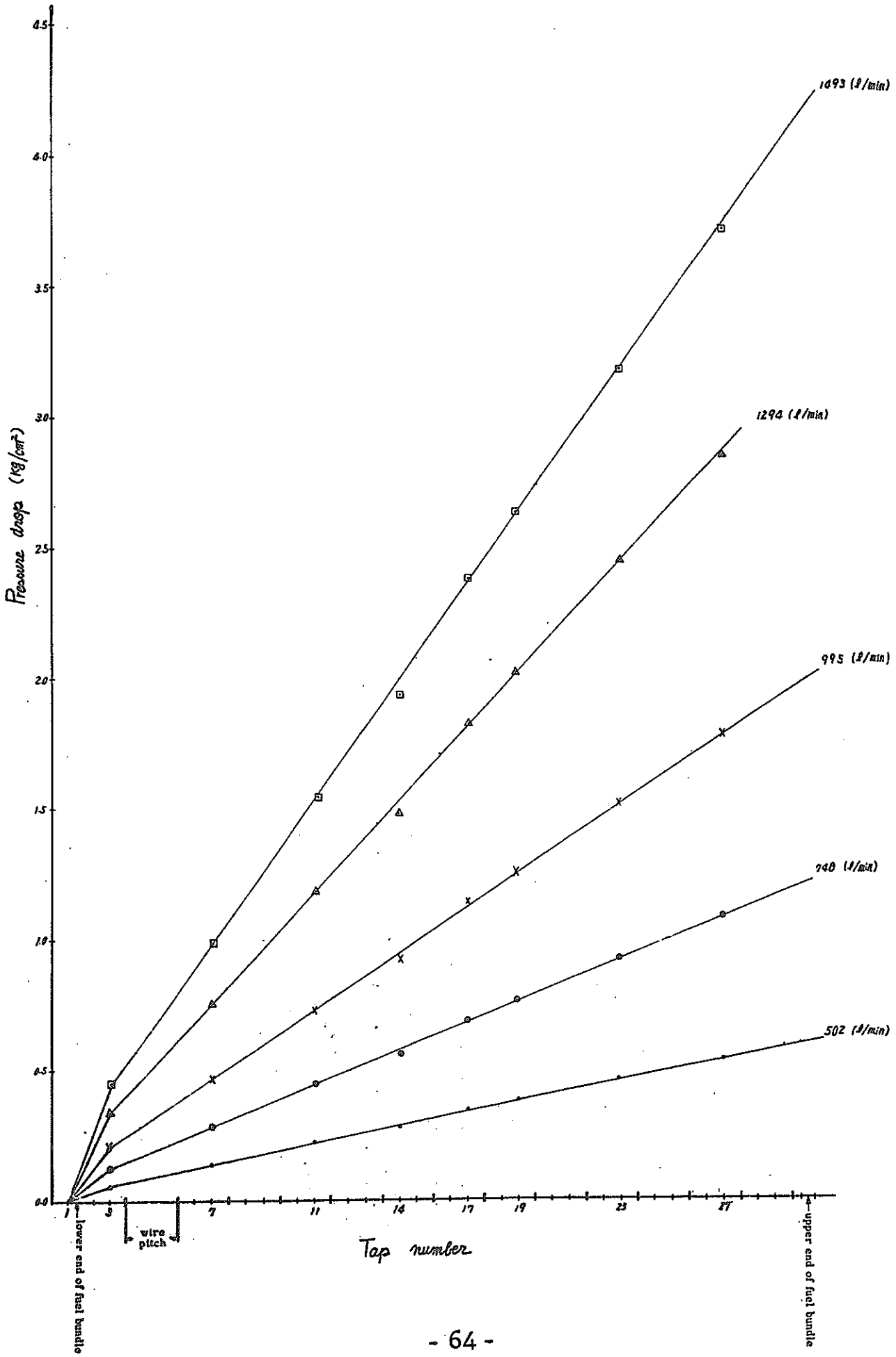

Fig. 32 Pressure drop on pin bundle (NFI (Sumitomo) wire type)

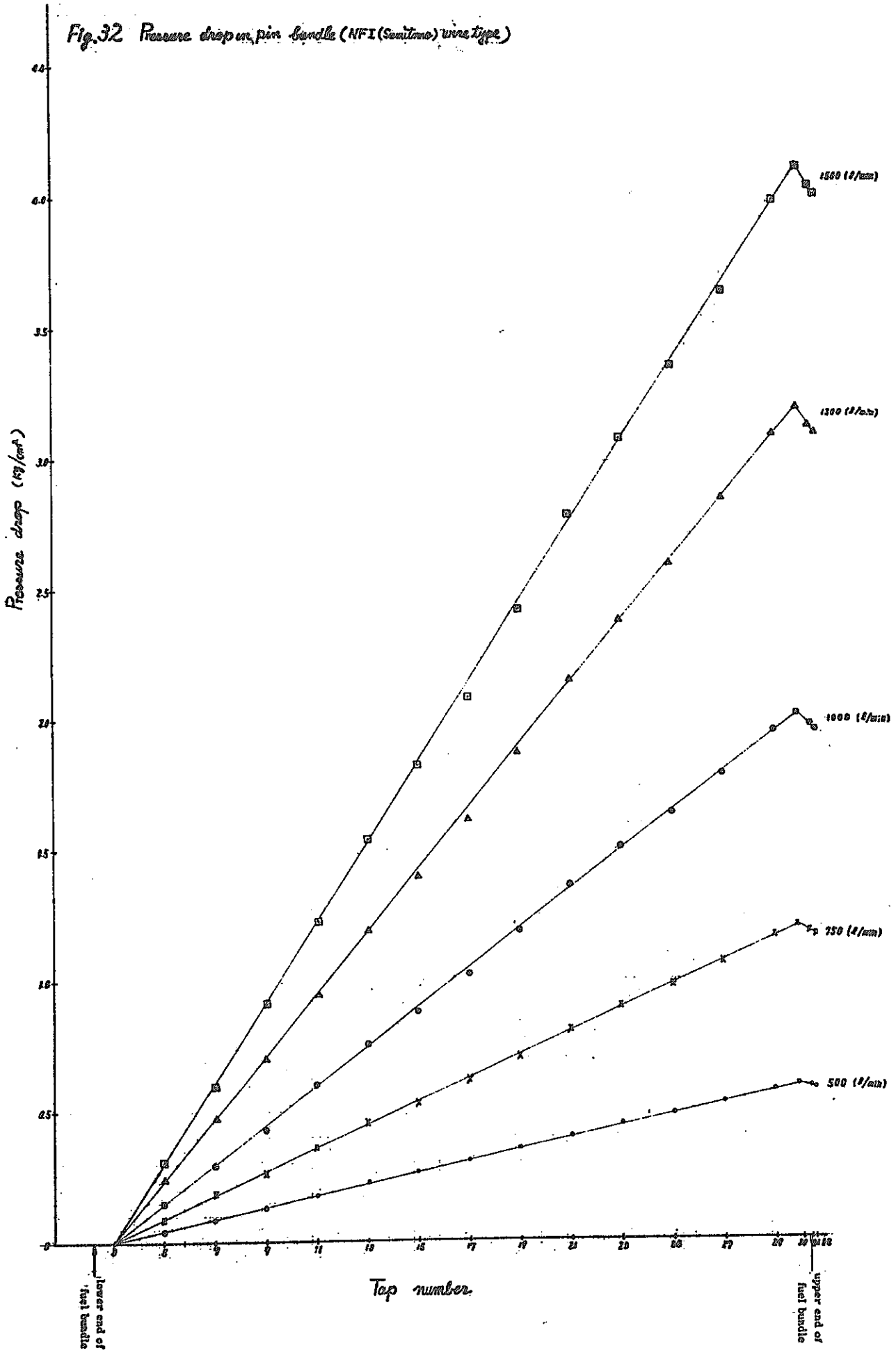

Fig. 33. Pressure Loss at Pin Bundle (Wire Wrap Type)

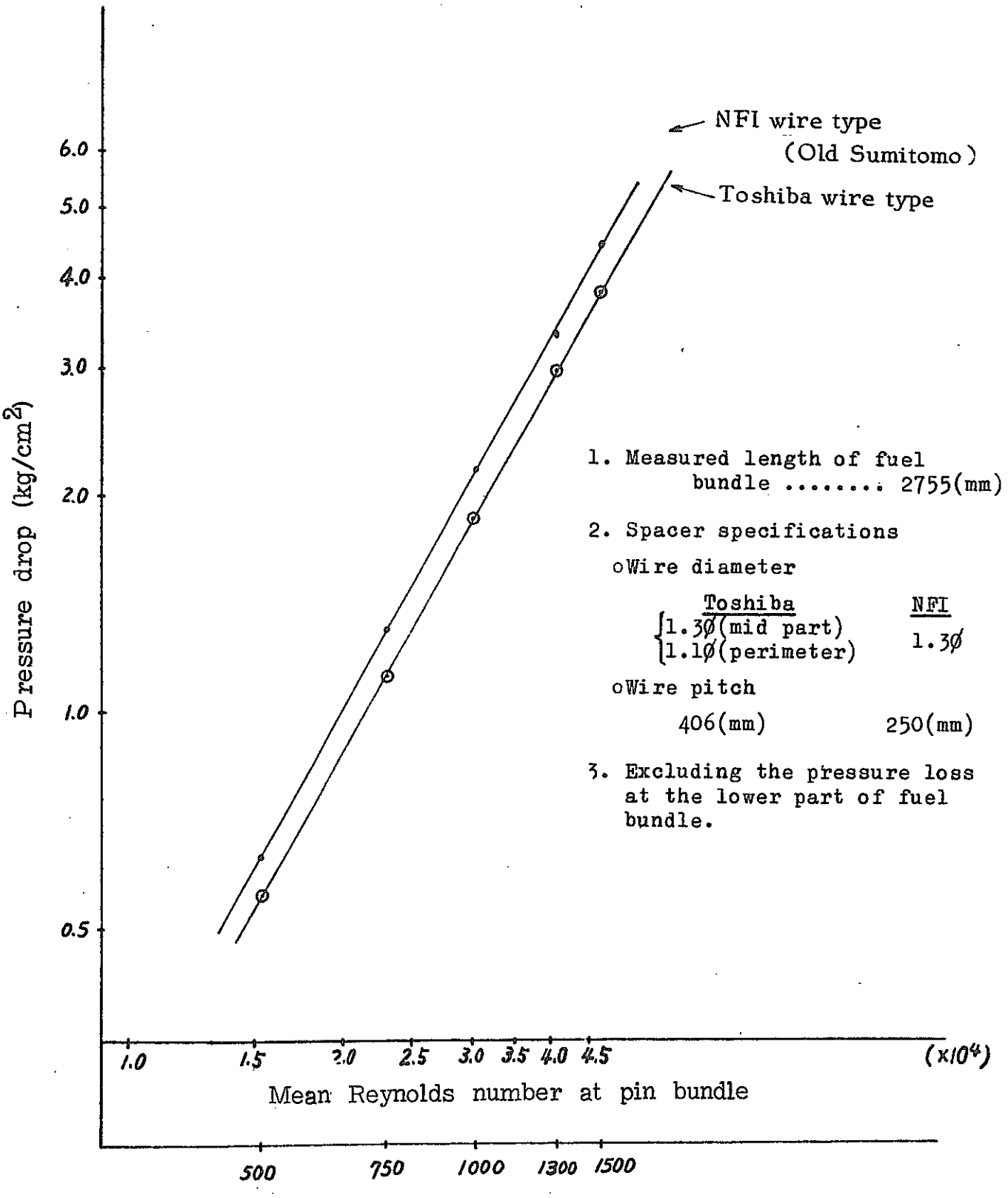

Fig. 34. Total Pressure Loss Excluding Pin Bundle (Grid Type) Breakdown of P

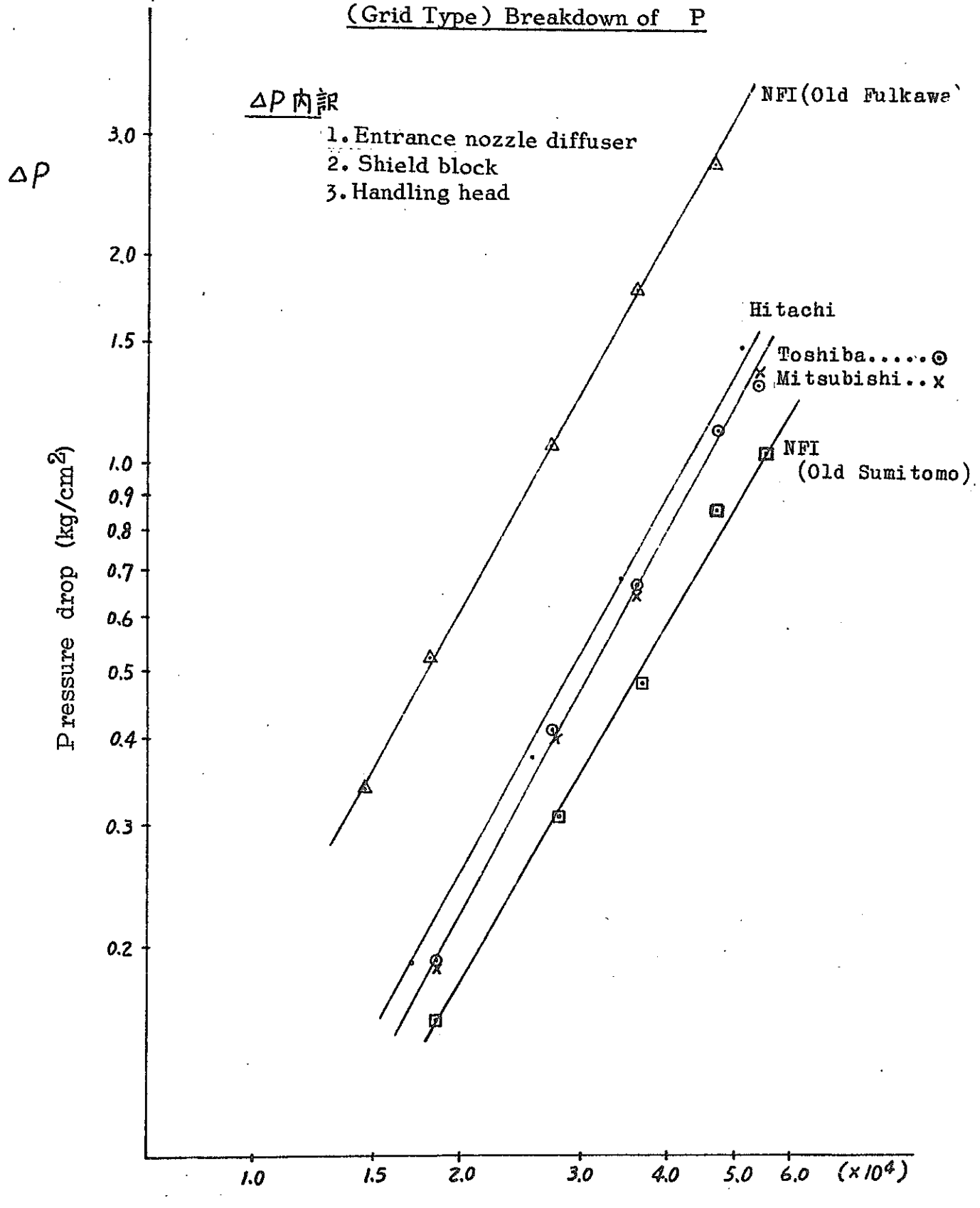

Fig. 35 The location of taps for pressure measurement (NFI (Sumitomo) blanket)

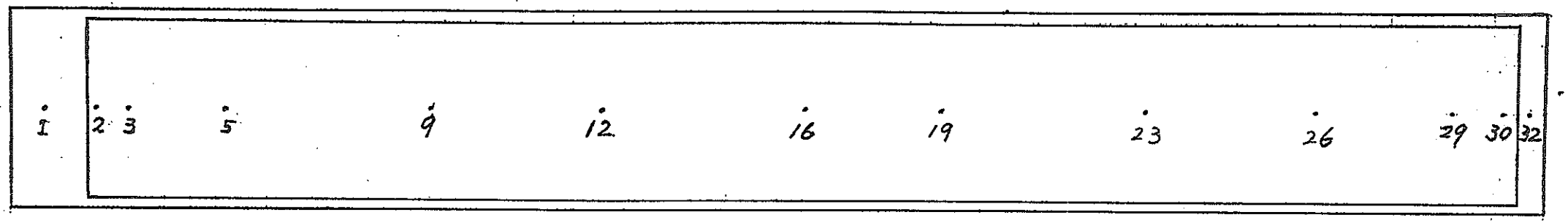

Tap No.	Place of Tap
1	63 (mm)
2	168
3	228
5	422
9	822
12	1155
16	1555
19	1822
23	2222
26	2555
29	2822
30	2923
32	2973

Fig. 36 Total pressure drop in blanket fuel assembly

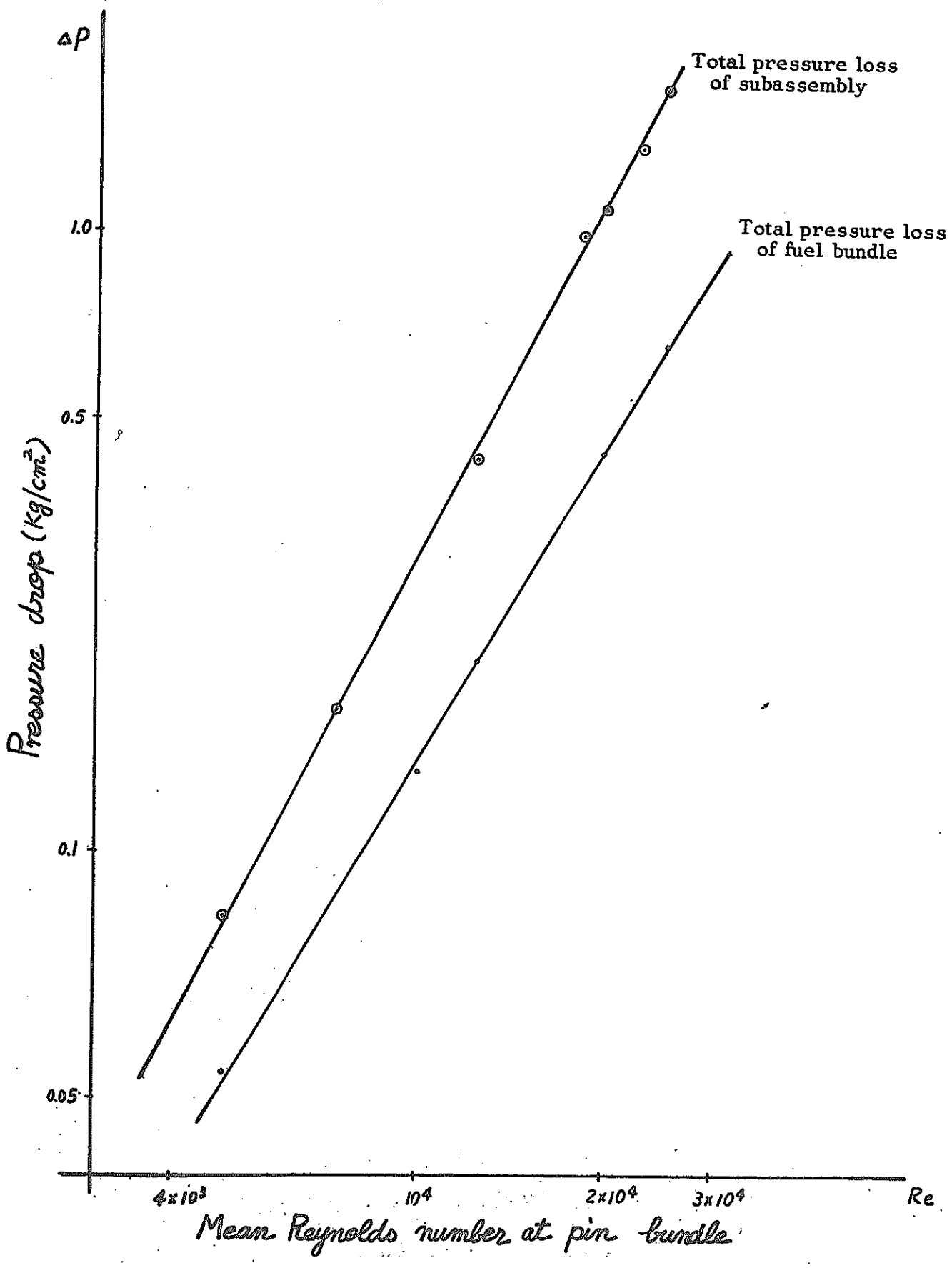

Fig.37 Pressure drop in pin bundle (NFI (Sumitomo) blanket)

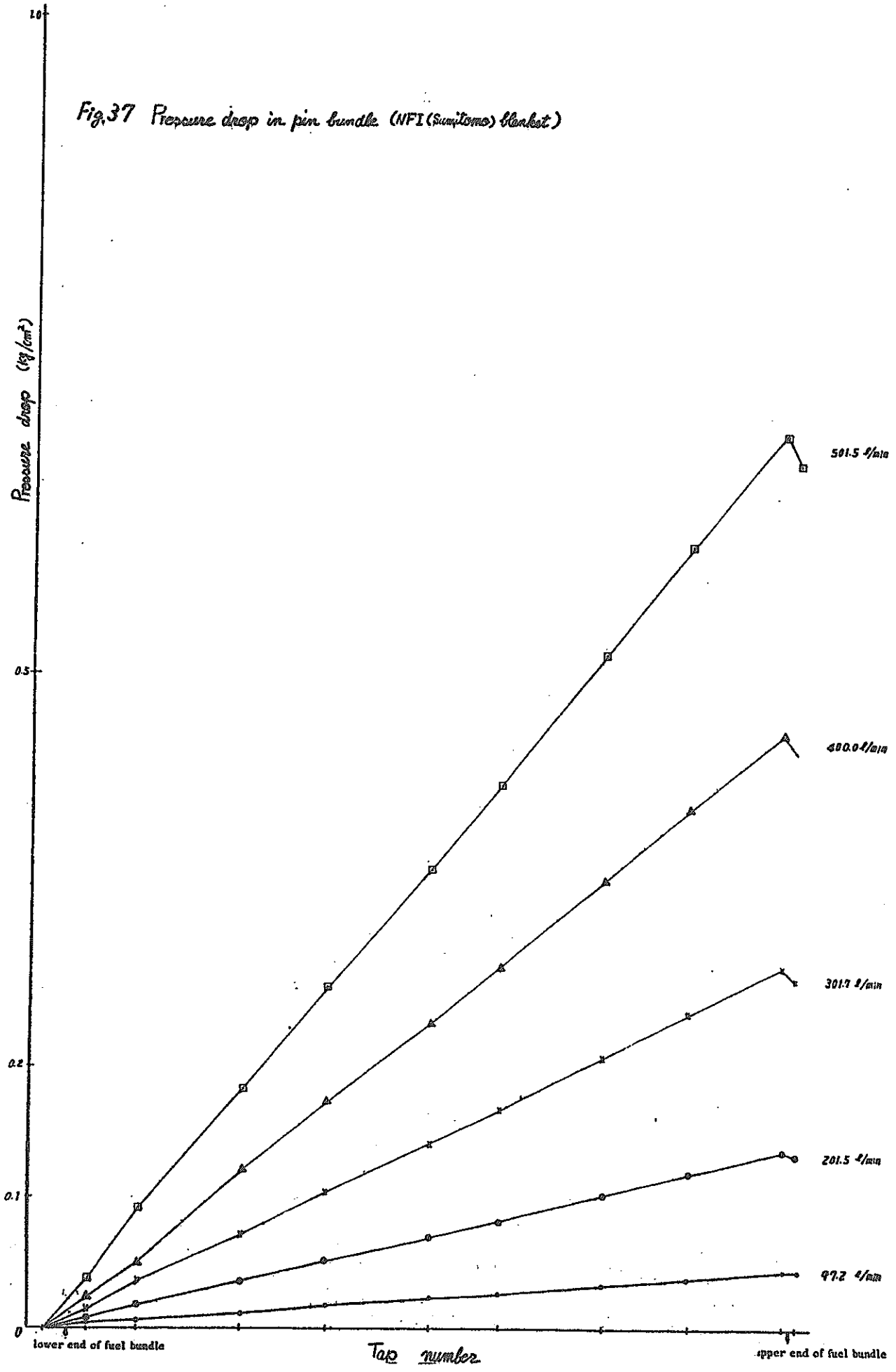

Fig. 38 Modified spacer loss coefficient

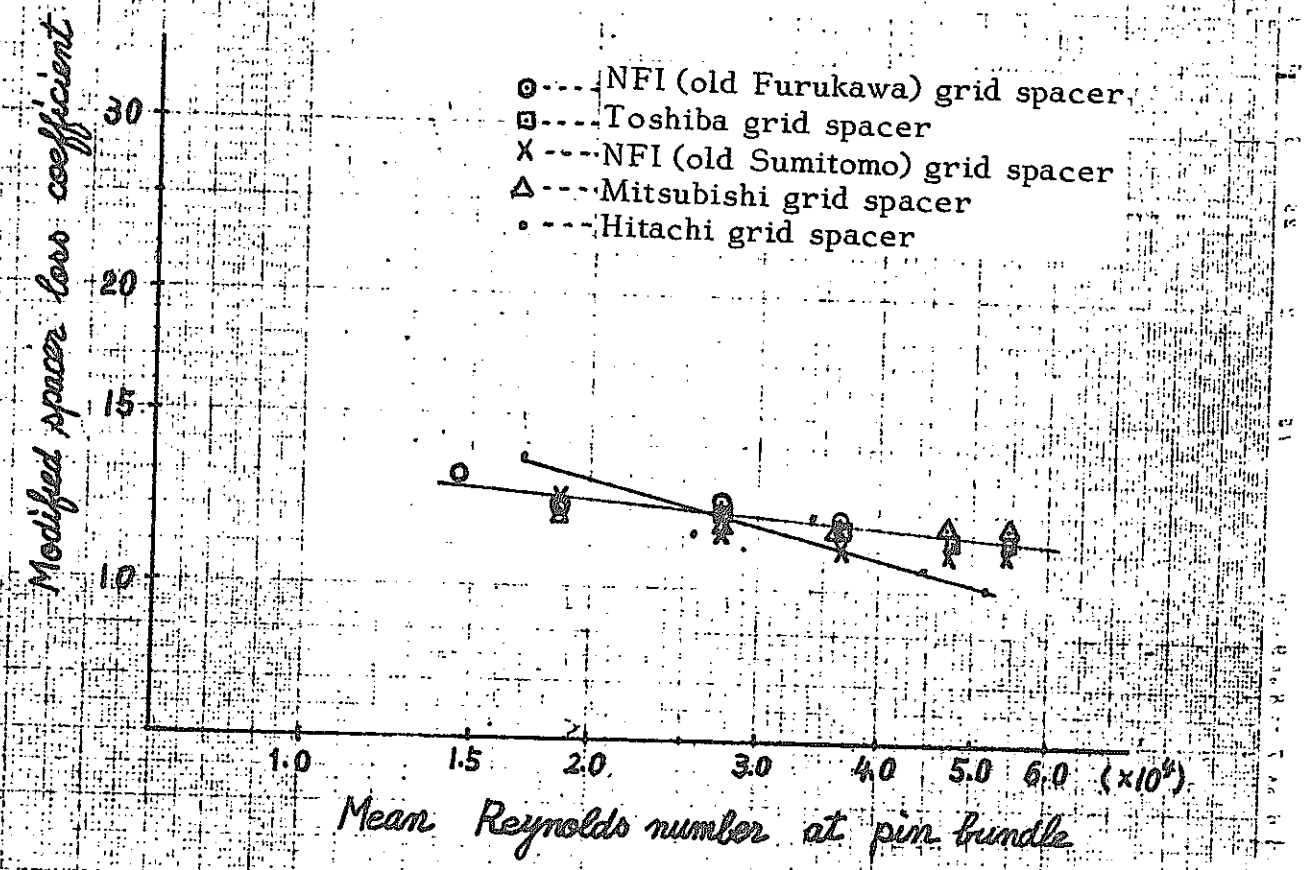

Fig. 39 Modified friction loss coefficient